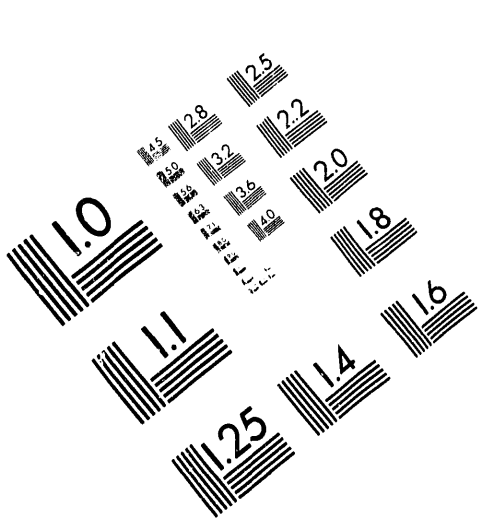

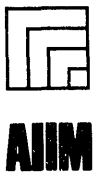

Association for Information and Image Management
1100 Wayne Avenue, Suite 1100
Silver Spring, Maryland 20910
301/587-8202

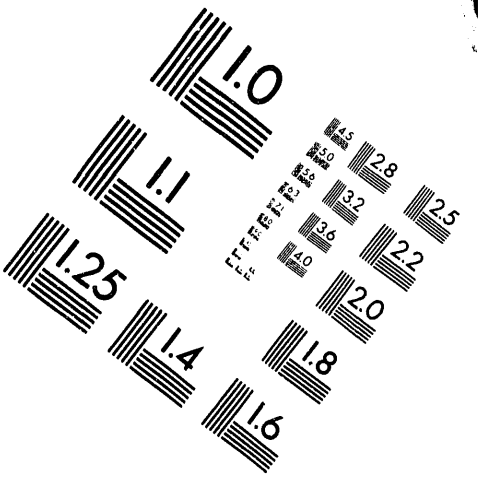

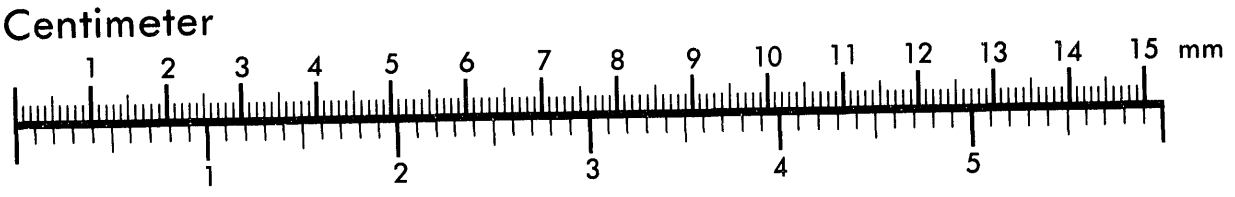

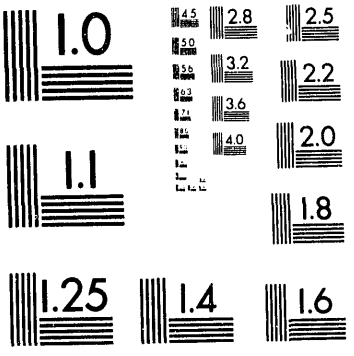

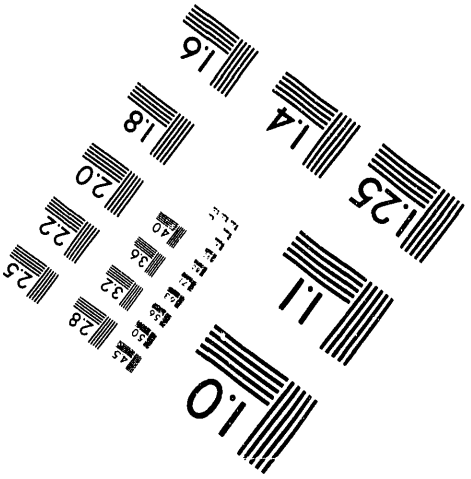

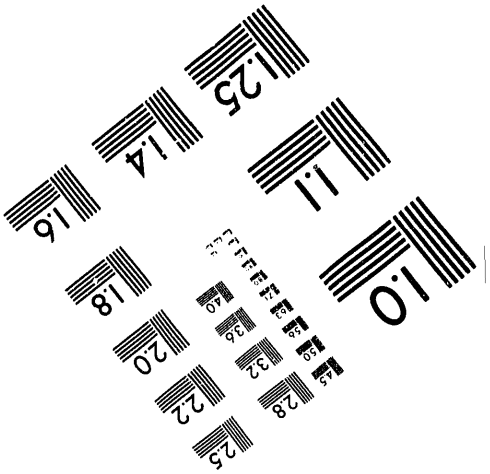

1 of 1

PREPARED FOR THE U.S. DEPARTMENT OF ENERGY,
UNDER CONTRACT DE-AC02-76-CHO-3073

PPPL-2911
UC-427

PPPL-2911

ANISOTROPIC ALFVÉN-BALLOONING MODES IN THE EARTH'S MAGNETOSPHERE

BY

A. A. CHAN, M. XIA AND L. CHEN

MAY, 1993

PPPL PRINCETON PLASMA PHYSICS LABORATORY

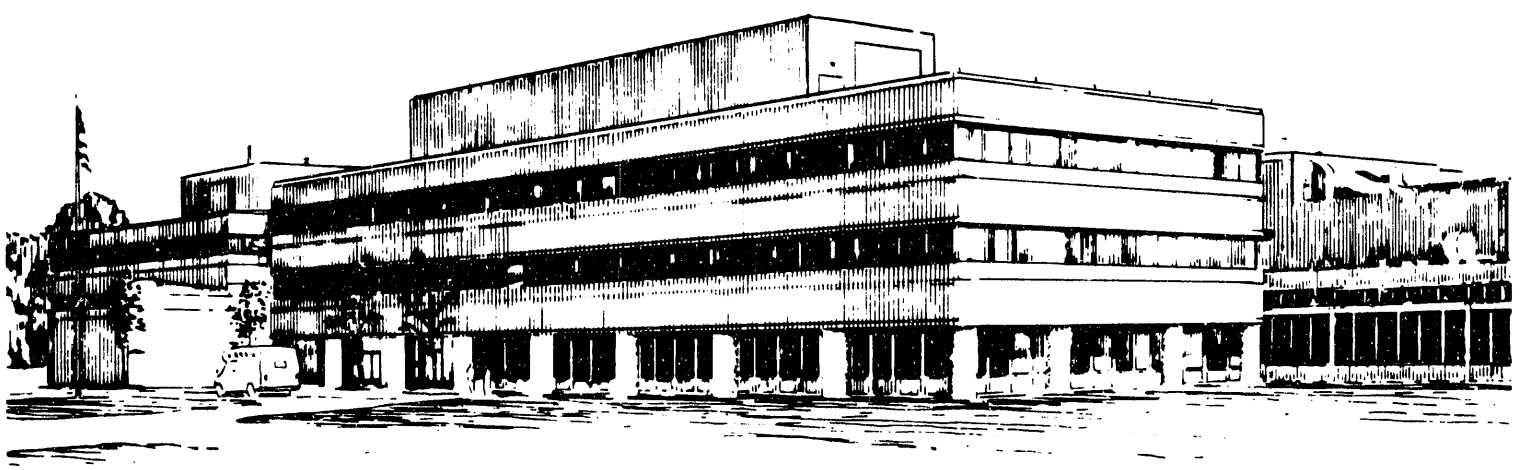

NOTICE

Anisotropic Alfvén-Ballooning Modes in the Earth's Magnetosphere

ANTHONY A. CHAN[1]

Department of Physics and Astronomy, Dartmouth College, Hanover, New Hampshire

MENGFEN XIA

Physics Department, Peking University, Beijing, People's Republic of China

LIU CHEN

Plasma Physics Laboratory and Department of Astrophysical Sciences, Princeton University, Princeton, New Jersey

We have carried out a theoretical analysis of the stability and parallel structure of coupled shear-Alfvén and slow-magnetosonic waves in the Earth's inner magnetosphere (ie., at equatorial distances between about five and ten Earth radii) including effects of finite anisotropic plasma pressure. Multiscale perturbation analysis of the anisotropic Grad-Shafranov equation yields an approximate self-consistent magnetohydrodynamic (MHD) equilibrium. This MHD equilibrium is used in the numerical solution of a set of eigenmode equations which describe the field line eigenfrequency, linear stability, and parallel eigenmode structure. We call these modes anisotropic Alfvén-ballooning modes. The main results are: (1) The field line eigenfrequency can be significantly lowered by finite pressure effects. (2) The parallel mode structure of the transverse wave components is fairly insensitive to changes in the plasma pressure but the compressional magnetic component can become highly peaked near the magnetic equator due to increased pressure, especially when $P_\perp > P_\parallel$ (here $P_\perp$ and $P_\parallel$ are the perpendicular and parallel plasma pressure). (3) For the isotropic ($P_\parallel = P_\perp = P$) case ballooning instability can occur when the ratio of the plasma pressure to the magnetic pressure, $\beta = P/(B^2/8\pi)$, exceeds a critical value $\beta_0^B \approx 3.5$ at the equator. (4) Compared to the isotropic case the critical beta value is lowered by anisotropy, either due to decreased field-line-bending stabilization when $P_\parallel > P_\perp$, or due to increased ballooning-mirror destabilization when

$P_\perp > P_{||}$. (5) We use a "β–δ stability diagram" to display the regions of instability with respect to the equatorial values of the parameters $\overline{\beta}$ and δ, where $\overline{\beta} = (1/3)(\beta_{||} + 2\,\beta_\perp)$ is an average beta value and $\delta = 1 - P_{||}/P_\perp$ is a measure of the plasma anisotropy. The diagram is divided into regions corresponding to the firehose, mirror and ballooning instabilities. It appears that observed values of the plasma pressure are below the critical value for the isotropic ballooning instability but it may be possible to approach a ballooning-mirror instability when $P_\perp/P_{||} \gtrsim 2$.

Submitted to *Journal of Geophysical Research (Space Physics)*, April 14, 1993.

CONTENTS

1 INTRODUCTION

Ballooning modes are hydromagnetic modes associated with a plasma pressure gradient which has a component in the same direction as the local magnetic curvature vector. In this situation the effect of the pressure gradient is destabilizing and is maximized when the wavenumber $k_\perp$ in the direction perpendicular to both the local magnetic field and the pressure gradient is large; the limit where $k_\perp \rightarrow \infty$ is called the ballooning limit. A ballooning instability results when the destabilizing effect is sufficiently strong to overcome stabilizing effects such as magnetic field line bending.

Ballooning modes have been considered in studies of magnetospheric hydromagnetic waves [*Pokhotelov et al.*, 1986; *Viñas and Madden*, 1986] and in studies of the magnetohydrodynamic (MHD) stability of the geomagnetic tail [*Miura et al.*, 1989; *Lee and Wolf*, 1992]. A recent theoretical analysis of ballooning modes in space plasmas [*Hameiri et al.*, 1991] included effects due to gravity and plasma rotation. However, all of these papers assumed isotropic plasma pressure whereas measurements show that the perpendicular pressure $P_\perp$ usually exceeds the parallel pressure $P_\parallel$, especially during magnetic storms [*Lui et al.*, 1987; *Lui and Hamilton*, 1992].

Motivated by these observations we have carried out a theoretical analysis of the effects of anisotropic plasma pressure on the stability and field-aligned structure of hydromagnetic modes in the Earth's magnetosphere. We focus on the region where the radial pressure gradient and the magnetic field line curvature are both Earthward (ie., on the outer edge of the ring current) and where we assume the magnetic field is approximately dipolar. This corresponds roughly to equatorial radial distances between about five and ten Earth radii. Although we restrict our analysis to this region our results should also be useful for a qualitative interpretation of the effects of anisotropy in the near-Earth geomagnetic tail.

Our formulation is based on the reduced gyrokinetic eigenmode equations of Chen and Hasegawa [1991]. These equations describe the linear stability of magnetospheric hydromagnetic waves including effects due to nonuniform anisotropic equilibria and due to kinetic effects such as finite ion gyroradius, magnetic trapping and wave-particle resonances. Chen

and Hasegawa have investigated the general qualitative properties of the eigenmode equations analytically, our goal is to obtain quantitative results by numerical solution of the eigenmode equations. In order to focus on the effects of anisotropic equilibria we neglect all kinetic effects. As well as being an interesting special case this is a useful intermediate step toward more general cases; for example, the anisotropic eigenmode results can be used to evaluate growth rates for wave-particle resonance instabilities [*Chan*, 1991]. The calculations in this paper are divided into two main parts: (i) an analytical calculation of a self-consistent magnetospheric equilibrium which includes finite anisotropic pressure effects and (ii) a numerical analysis of the linear stability of the equilibrium. As we will see, the modes we consider are shear-Alfvén waves and slow-magnetosonic waves which are coupled by the inhomogeneity of the pressure and the magnetic field; following Chen and Hasegawa we call these modes anisotropic Alfvén-ballooning modes.

The remainder of this paper is organized as follows: First we introduce the anisotropic MHD equilibrium equations, describe a theoretical plasma model for the inner magnetosphere, and use multiscale perturbation methods to obtain an approximate equilibrium solution. The equilibrium solution is then used to obtain numerical solutions of the eigenmode equations of Chen and Hasegawa. The isotropic pressure case is considered first, followed by a study of the effects of anisotropy. The results presented include plots of the field-aligned structure of the anisotropic Alfvén-ballooning modes and the corresponding field line eigenfrequencies and stability limits. The final section gives a summary and discussion of the main results of this paper. The appendix contains a description of the computer code used to solve the eigenmode equations.

2 ANISOTROPIC MHD EQUILIBRIUM

2.1 Theoretical Model

Following Chen and Hasegawa [1991] the equilibrium magnetic field is represented as

$$\mathbf{B} = \nabla\psi \times \nabla\phi\,, \tag{1}$$

where ψ is the poloidal magnetic flux coordinate and ϕ is the azimuthal symmetry angle. We assume the magnetospheric plasma is collisionless with $\mu = v_\perp^2/2B$, $\varepsilon = v^2/2$, and ψ constants of the motion. Here $v_\perp$ is the particle velocity perpendicular to the magnetic field, $B = |\mathbf{B}|$ is the magnitude of the local magnetic field, μ is the magnetic moment per unit mass, and ε is the particle energy per unit mass. To within constant factors and small terms μ is equal to the first adiabatic invariant and ψ is proportional to the third adiabatic invariant, ie., the flux linked by the particle due to its ∇B and curvature drifts [*Northrop*, 1963].

Note that any equilibrium distribution function $F_0 = F_0(\mu, \varepsilon, \psi)$ is automatically a solution of the corresponding Vlasov equation. Furthermore, the equilibrium pressure tensor P is gyrotropic; ie.,

$$\mathsf{P} = P_\perp \mathsf{I} + (P_\parallel - P_\perp)\mathbf{bb}\,, \tag{2}$$

where I is the unit tensor and $\mathbf{b} = \mathbf{B}/B$ is a unit vector in the direction of the local magnetic field, and the diagonal elements have the following form:

$$P_\parallel = \sum_{\hat{\sigma}} 2\pi M \int_0^\infty d\varepsilon \int_0^{\varepsilon/B} \frac{B\,d\mu}{\sqrt{2(\varepsilon - \mu B)}}\, 2(\varepsilon - \mu B)\, F_0(\mu, \varepsilon, \psi)\,, \tag{3}$$

$$P_\perp = \sum_{\hat{\sigma}} 2\pi M \int_0^\infty d\varepsilon \int_0^{\varepsilon/B} \frac{B\,d\mu}{\sqrt{2(\varepsilon - \mu B)}}\, \mu B\, F_0(\mu, \varepsilon, \psi)\,. \tag{4}$$

Here the sum over $\hat{\sigma} = v_\parallel/|v_\parallel|$ denotes a sum over both directions of the parallel velocity, M is the particle mass, and we have suppressed the sum over plasma species.

Consistent with our theoretical model of the magnetospheric plasma we note that axisymmetric anisotropic MHD equilibrium is governed by the following two equations [*Hasegawa*

and Sato, 1989; *Cheng,* 1992]:

$$B\left(\frac{\partial P_{||}}{\partial B}\right)_{\psi} = P_{||} - P_{\perp}\,, \tag{5}$$

which describes parallel MHD force balance, and

$$\sigma\Delta^{*}\psi + \nabla\sigma\cdot\nabla\psi + 4\pi R^{2}\left(\frac{\partial P_{||}}{\partial\psi}\right)_{B} = 0\,, \tag{6}$$

which describes perpendicular MHD force balance. Here

$$\sigma = 1 - \frac{4\pi}{B}\left(\frac{\partial P_{||}}{\partial B}\right)_{\psi} \tag{7}$$

is the firehose instability parameter ($\sigma < 0$ implies firehose instability) and Δ^{*} is an elliptic differential operator which is defined as follows in cylindrical coordinates (R, ϕ, Z):

$$\Delta^{*} = \frac{\partial^{2}}{\partial R^{2}} - \frac{1}{R}\frac{\partial}{\partial R} + \frac{\partial^{2}}{\partial Z^{2}}\,. \tag{8}$$

Note that the parallel and perpendicular pressure $P_{||}$ and $P_{\perp}$ are regarded as functions of ψ and $B = |\mathbf{B}|$.

Using equation (5) and the definition of the firehose parameter σ, equation (7), we have

$$\sigma = 1 + \frac{1}{2}\left(\beta_{\perp} - \beta_{||}\right), \tag{9}$$

where $\beta_{||} = 8\pi P_{||}/B^{2}$ and $\beta_{\perp} = 8\pi P_{\perp}/B^{2}$ are ratios of the plasma pressure to the magnetic pressure.

In the isotropic limit $P_{||} = P_{\perp} = P$ equation (5) implies the well-known isotropic MHD result that the pressure is constant along a magnetic field line and equation (6) reduces to the Grad-Shafranov equation [*Freidberg,* 1982]. We refer to equation (6) as the anisotropic Grad-Shafranov equation.

2.2 Parallel Force Balance

Direct substitution of equations (3) and (4) into equation (5) shows that parallel force balance is automatically satisfied when the equilibrium distribution function F_0 is a function

of (μ, ε, ψ). To proceed further we must adopt a functional form for F_0. For simplicity we choose a bi-maxwellian distribution function

$$F_0(\mu,\varepsilon,\psi) = \begin{cases} \dfrac{n_0}{T_{\|0}^{1/2} T_{\perp 0}} \left(\dfrac{M}{2\pi}\right)^{3/2} \exp\left[-\dfrac{M(\varepsilon-\mu B_0)}{T_{\|0}} - \dfrac{M\mu B_0}{T_{\perp 0}}\right] & \text{for } \mu \le \varepsilon/B\ , \\ 0 & \text{for } \mu > \varepsilon/B\ . \end{cases} \tag{10}$$

Here $n_0(\psi)$, $T_{\|0}(\psi)$, $T_{\perp 0}(\psi)$, and $B_0(\psi)$ are the number density, parallel temperature, perpendicular temperature, and magnetic field, where the subscript zero denotes quantities evaluated at the equator. The parallel and perpendicular pressures at the equator are given by $P_{\|0} = n_0 T_{\|0}$ and $P_{\perp 0} = n_0 T_{\perp 0}$.

We define the anisotropy parameter

$$\delta = 1 - \frac{P_\|}{P_\perp}\ . \tag{11}$$

Note that observations [*Lui et al.*, 1987] typically show $P_\perp \ge P_\|$ which corresponds to $0 \le \delta < 1$ or "positive" anisotropy.

Substituting the bi-maxwellian, equation (10), into equations (3) and (4) gives $P_\|$ and $P_\perp$ explicitly as functions of ψ and B, as follows:

$$P_\| = P_{\|0}\left(\frac{1-\delta_0}{1-\delta_0 B_0/B}\right), \tag{12}$$

$$P_\perp = P_{\perp 0}\left(\frac{1-\delta_0}{1-\delta_0 B_0/B}\right)^2, \tag{13}$$

where $\delta_0 = 1 - P_{\|0}/P_{\perp 0}$. Then we have

$$\delta = \delta_0 \frac{B_0}{B}, \tag{14}$$

$$\beta_\| = \frac{8\pi P_\|}{B^2} = \beta_{\|0}\left(\frac{B_0}{B}\right)^2\left(\frac{1-\delta_0}{1-\delta}\right), \tag{15}$$

and

$$\beta_\perp = \frac{8\pi P_\perp}{B^2} = \beta_{\perp 0}\left(\frac{B_0}{B}\right)^2\left(\frac{1-\delta_0}{1-\delta}\right)^2, \tag{16}$$

where $\beta_{\|0} = 8\pi P_{\|0}/B^2$ and $\beta_{\perp 0} = 8\pi P_{\perp 0}/B^2$ are the beta values at the equator. Equations (12) and (13) are in agreement with the corresponding results given recently by C. Z. Cheng [1992].

In the isotropic limit ($\delta \rightarrow 0$) equations (15) and (16) reduce to the expected form

$$\beta = \frac{8\pi P}{B^2} = \beta_0 \left(\frac{B_0}{B}\right)^2 \tag{17}$$

where $\beta_0 = 8\pi P/B_0^2$. In contrast to the isotropic case, where the pressure P is independent of B, from equations (12)–(17) we see that the quantities $P_{\|}$, $P_{\perp}$, δ, $\beta_{\|}$ and $\beta_{\perp}$ all decrease with increasing B. Furthermore, the decrease of $\beta_{\|}$ and $\beta_{\perp}$ with increasing B is faster than that of the isotropic beta value and is faster with higher anisotropy δ.

For a more quantitative comparison with the isotropic case we define an average beta value

$$\overline{\beta} = \frac{1}{3}\left(\beta_{\|} + 2\beta_{\perp}\right). \tag{18}$$

In the isotropic limit $\overline{\beta} = \beta$. In Figure 1 we use equations (15) and (16) to plot the average beta value evaluated along a magnetic field line for three values of the equatorial anisotropy δ_0. For simplicity we assume the equilibrium magnetic field is a magnetic dipole. For $\delta_0 = 0$, $\delta_0 = 0.5$, and $\delta_0 = 0.9$ the full-width-at-half-maximum of the corresponding average beta decreases from 33° to 25° to 11°, respectively. We will see that this increased equatorial localization due to increased anisotropy results in hydromagnetic wave amplitudes which are strongly peaked near the magnetic equator.

2.3 Perpendicular Force Balance

Recall that the equilibrium magnetic field is represented as $\mathbf{B} = \nabla\psi \times \nabla\phi$ where ψ satisfies the anisotropic Grad-Shafranov equation, equation (6). In principle, once $P_{\|}(\psi, B)$, $P_{\perp}(\psi, B)$, and boundary conditions are specified equation (6) can be solved numerically (see [*Cheng,* 1992], for example). However, because the eigenmode analysis of Chen and Hasegawa [1991] is essentially a local analysis valid near a given field line, we adopt a *local* multiscale perturbation method [*Bender and Orszag,* 1978] of solving equation (6). This

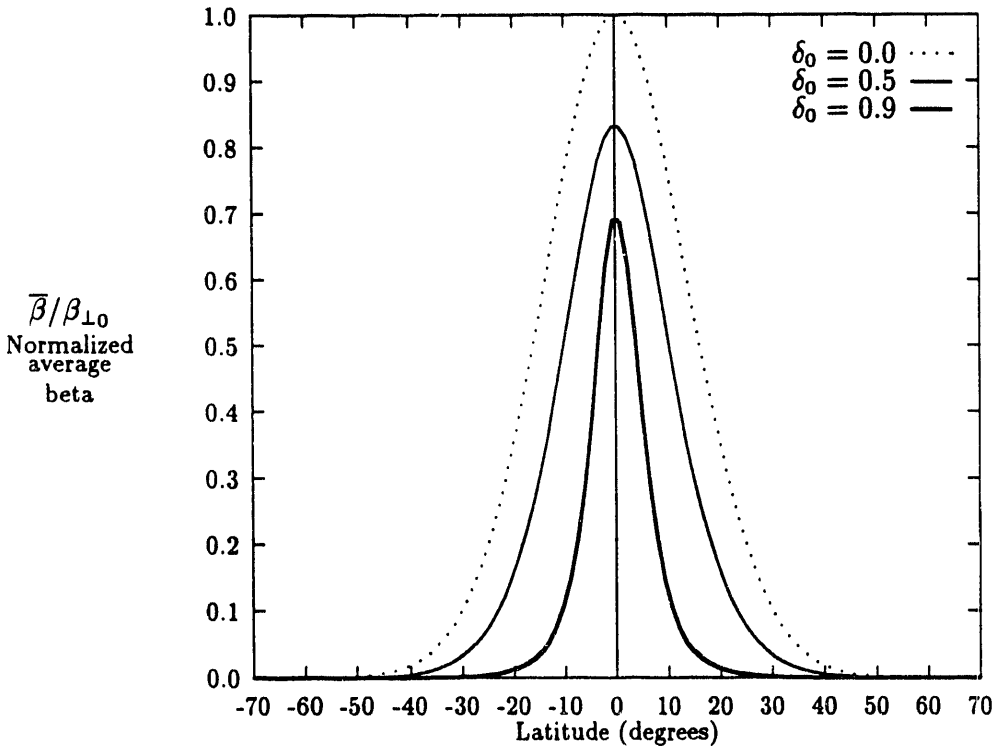

Figure 1: Average beta $\overline{\beta} = (1/3)(\beta_{||} + 2\beta_{\perp})$ evaluated along a magnetic field line and normalized to the equatorial value $\beta_{\perp 0}$, for three values of the equatorial anisotropy $\delta_0 = 1 - P_{||0}/P_{\perp 0}$. This plot assumes a magnetic dipole equilibrium field. Note the increase in equatorial localization as the anisotropy is increased.

approach is much less laborious than a numerical solution and has the advantage of yielding a simple analytic formula for the equilibrium magnetic field.

We begin by rewriting equation (6) as

$$\sigma \Delta^* \psi = -4\pi R^2 \left[\left(\frac{\partial P_\perp}{\partial \psi} \right)_l + \left(\frac{\partial P_\parallel}{\partial B} \right)_\psi \left(\frac{\partial B}{\partial \psi} \right)_l \right], \tag{19}$$

where l is the distance along the field line measured from the equator and we have explicitly indicated which variables are to be held constant in the partial derivatives. In deriving equation (19) we used the chain rule and the relations $\nabla\psi \cdot \nabla l = 0$, $|\nabla l|^2 = 1$, and $|\nabla\psi|^2 = R^2 B^2$.

The effects of finite pressure are assumed to be a small perturbation on a given vacuum (pressureless) equilibrium, thus we formally order $\beta_\perp = \mathcal{O}(\epsilon_\beta)$, where $\epsilon_\beta \ll 1$ is a small parameter. Furthermore, because the Alfvén-ballooning instability is driven by a steep radial pressure gradient [*Chen and Hasegawa,* 1991], we assume the pressure gradient scale length is small compared to the local magnetic field scale length; specifically, we assume $|\partial \ln P_{\parallel 0}/\partial\psi| = |\partial \ln P_{\perp 0}/\partial\psi| = \alpha/\psi_0$ in the vicinity of a given flux surface $\psi = \psi_0$, where $\alpha = \mathcal{O}(\epsilon_\beta^{-1})$ is a measure of the steepness of the radial pressure gradient. With these orderings the multiscale perturbation methods allow us to separate the effects of the steep radial pressure gradient from effects due to the inhomogeneity of the equilibrium field.

As the zero-order ($\epsilon_\beta = 0$) approximation we adopt the vacuum dipole field, given by $\mathbf{B}_V = \nabla\psi_V \times \nabla\phi$, where ψ_V satisfies

$$\Delta^* \psi_V = 0. \tag{20}$$

In cylindrical coordinates $\psi_V = \mathcal{B}_E \mathcal{R}_E{}^3 R^2/(R^2 + Z^2)^{3/2}$, where $\mathcal{B}_E = 0.31$ gauss is the magnetic field strength at one Earth radius $\mathcal{R}_E = 6380$ km.

Selecting coordinates (ψ_V, l_V), where l_V is the distance along the vacuum dipole field line measured from the equator, the factor $\Delta^* \psi$ on the left hand side of equation (19) becomes

$$\Delta^* \psi = R^2 B_V^2 \left(\frac{\partial^2 \psi}{\partial \psi_V{}^2} \right)_{l_V} + \left(\frac{\partial^2 \psi}{\partial l_V{}^2} \right)_{\psi_V} + \left(\frac{\partial \psi}{\partial l_V} \right)_{\psi_V} \Delta^* l_V, \tag{21}$$

where we have used equation (20) and the relations $\nabla\psi_V \cdot \nabla l_V = 0$, $|\nabla l_V|^2 = 1$, and $|\nabla\psi_V|^2 = R^2 B_V^2$.

The right hand side of equation (19) contains derivatives of the pressure along the field line, so we now consider the orderings of the parallel length scales of $P_\perp$, $P_\parallel$, and B near the equator, denoted by $l_{P_\perp}$, $l_{P_\parallel}$, and l_B. Consider $l_{P_\perp}$ first. Since $P_\perp$ and B are even functions of l we have

$$P_\perp(\psi, l) \approx P_{\perp 0} + \tfrac{1}{2} P_\perp{}'' \, l^2 \tag{22}$$

$$B(\psi, l) \approx B_0 + \tfrac{1}{2} B'' \, l^2 \tag{23}$$

near the equator, where the prime denotes a derivative with respect to l. Then, defining l_B by $B'' = B_0/{l_B}^2$ and $l_{P_\perp}$ by $P_\perp{}'' = P_{\perp 0}/{l_{P_\perp}}^2$, we have

$$\frac{1}{B}\left(\frac{\partial P_\perp}{\partial B}\right)_\psi = \frac{1}{B}\left(\frac{\partial P_\perp}{\partial l}\right)_\psi \left(\frac{\partial l}{\partial B}\right)_\psi \approx \frac{1}{B}\frac{P_\perp{}'' l}{B'' l} \sim \beta_{\perp 0}\frac{{l_B}^2}{{l_{P_\perp}}^2}\,, \tag{24}$$

or

$$\frac{{l_{P_\perp}}^2}{{l_B}^2} \sim \beta_{\perp 0}\left[\frac{1}{B}\left(\frac{\partial P_\perp}{\partial B}\right)_\psi\right]^{-1}. \tag{25}$$

Similarly, for $l_{P_\parallel}$ we have

$$\frac{{l_{P_\parallel}}^2}{{l_B}^2} \sim \beta_{\parallel 0}\left[\frac{1}{B}\left(\frac{\partial P_\parallel}{\partial B}\right)_\psi\right]^{-1}. \tag{26}$$

Two cases are treated, corresponding to magnetospheric plasma with "mild" or "strong" anisotropy. For the mild anisotropy case, defined by

$$(1 - \delta_0) \sim 1/2\,, \tag{27}$$

we have $\beta_{\parallel 0} \sim \beta_{\perp 0} = \mathcal{O}(\epsilon_\beta)$, $(1/B)(\partial P_\perp/\partial B)_\psi \sim (1/B)(\partial P_\parallel/\partial B)_\psi \sim \mathcal{O}(\epsilon_\beta)$, and from equations (25) and (26)

$$l_{P_\parallel}/l_B \sim l_{P_\perp}/l_B = \mathcal{O}(\epsilon_\beta^0)\,. \tag{28}$$

However, for the strong anisotropy case, defined by

$$(1 - \delta_0) \sim \mathcal{O}(\epsilon_\beta)\,, \tag{29}$$

we have $\beta_{\|_0} = \mathcal{O}(\epsilon_\beta^2)$, $\beta_{\perp 0} = \mathcal{O}(\epsilon_\beta)$, $(1/B)(\partial P_\perp/\partial B)_\psi \sim \mathcal{O}(1)$, $(1/B)(\partial P_\|/\partial B)_\psi \sim \mathcal{O}(\epsilon_\beta)$, and

$$l_{P_\|}/l_B \sim l_{P_\perp}/l_B \sim \mathcal{O}(\epsilon_\beta^{1/2}) \,. \tag{30}$$

Now consider the radial pressure variation. For the purpose of the multiscale perturbation expansion we consider a local pressure "bump" at some particular value $\psi = \psi_0$ as sketched in Figure 2, and we will explicitly label functions such as $P_\perp$ by their order in ϵ_β. It will

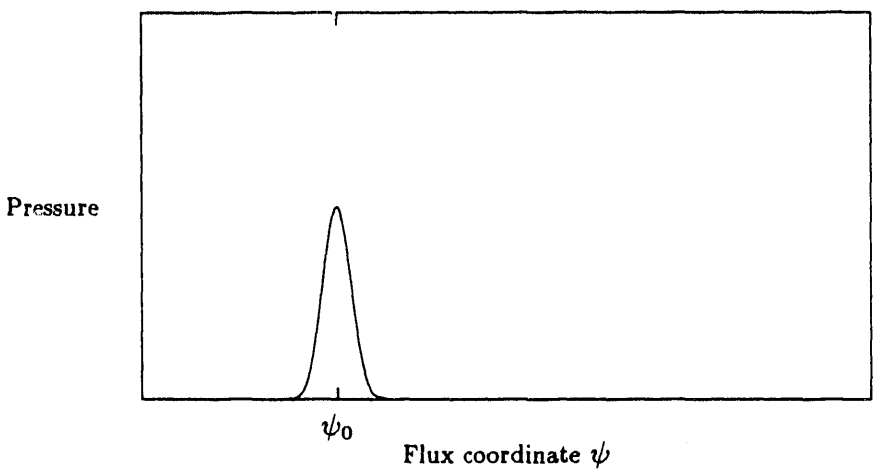

Figure 2: Sketch of the pressure perturbation $P_\|(\psi)$ or $P_\perp(\psi)$.

also be convenient to label the function arguments by some power of ϵ_β which denotes whether the function varies slowly or rapidly with respect to that argument. For example, since $\beta_\perp \sim \epsilon_\beta$ and $|\partial \ln P_\perp/\partial\psi| \sim \epsilon_\beta^{-1}/\psi_0$ we write $\epsilon_\beta P_\perp(\epsilon_\beta^{-1}\tilde{\psi})$ where $\tilde{\psi} = \psi - \psi_0$; this notation reflects the fact that the derivative $\partial/\partial\psi$ yields a factor of ϵ_β^{-1} which denotes the fast radial variation of the pressure.

For the mild anisotropy case we expand the solution $\psi(\psi_V, l_V)$ as follows:

$$\psi(\psi_V, l_V) = \psi_V + \sum_{n=1}^{\infty} \epsilon_\beta^n \, \psi_n\left(\epsilon_\beta^{-1}\tilde{\psi}, \epsilon_\beta^0 l_V\right) \,. \tag{31}$$

In equation (31) the argument $\epsilon_\beta^0 l_V$ represents the orderings of equation (28) and ψ_V,

$\epsilon_\beta^{-1}\tilde{\psi}$ and $\epsilon_\beta^0 l_V$ are regarded as independent variables in the multiscale expansion. We substitute equation (31) into equations (21) and (19), use the orderings $\epsilon_\beta^1 P_\parallel$, $\epsilon_\beta^1 P_\perp$, $\epsilon_\beta^1(\partial P_\parallel/\partial B)_\psi(\partial B/\partial\psi)_l$, and $\epsilon_\beta^0(\partial P_\perp/\partial\psi)_l$, and expand order by order in ϵ_β. To order ϵ_β^{-1}, $\partial^2\psi_1/\partial\psi_V^2 = 0$ and we choose $\psi_1 = 0$. To order ϵ_β^0 we have

$$\left(\frac{\partial^2\psi_2}{\partial{\psi_V}^2}\right)_{l_V} = -\frac{4\pi}{B_V^2}\left(\frac{\partial P_\perp}{\partial\psi_V}\right)_{l_V}, \tag{32}$$

or, integrating once with respect to the fast flux variable,

$$\left(\frac{\partial\psi_2}{\partial\psi_V}\right)_{l_V} = -\frac{1}{2}\beta_{\perp V}, \tag{33}$$

where $\beta_{\perp V} = 8\pi P_\perp/B_V^2$. Using equation (1) and $\psi = \psi_V + \psi_2 + \mathcal{O}(\epsilon_\beta^3)$, we have

$$\mathbf{B} = \mathbf{B}_V\,(1 - \beta_{\perp V}/2) + \mathcal{O}(\epsilon_\beta^2)\,, \tag{34}$$

which is the desired expression for the equilibrium magnetic field.

Similarly, for the strong anisotropy case equations (29)–(30) suggest that the local perturbation expansion should be of the form:

$$\psi(\psi_V, l_V) = \psi_V + \sum_{n=1}^{\infty}\epsilon_\beta^{n/2}\psi_{n/2}\left(\epsilon_\beta^{-1}\psi_V, \epsilon_\beta^{-1/2}l_V\right)\,. \tag{35}$$

In this case we set $\psi_{1/2} = \psi_1 = \psi_{3/2} = 0$ at orders $\epsilon_\beta^{-3/2}$, ϵ_β^{-1}, and $\epsilon_\beta^{-1/2}$, respectively, and obtain

$$\left(\frac{\partial\psi_2}{\partial\psi_V}\right)_{l_V} = -\frac{1}{2}\beta_{\perp V}, \tag{36}$$

at order ϵ_β^0, as in equation (33). Then

$$\mathbf{B} = \mathbf{B}_V\,(1 - \beta_{\perp V}/2) + \mathcal{O}(\epsilon_\beta^{3/2}), \tag{37}$$

which, apart from high-order neglected terms, has the same form as equation (34).

So, for either mild or strong anisotropy the modification of the dipole magnetic field due to finite anisotropic pressure is given approximately by

$$\mathbf{B} = \mathbf{B}_V\,(1 - \beta_{\perp V}/2)\,. \tag{38}$$

Thus, to order ϵ_β the field lines are parallel with those of the vacuum dipole field but the magnitude of the local magnetic field is depressed by the diamagnetic effect due to the finite perpendicular pressure. For later use note that the field line distance l and the field line curvature $\boldsymbol{\kappa} = \mathbf{b} \cdot \nabla \mathbf{b}$ differ from the corresponding dipole values by terms of order ϵ_β^2. Analogous results for the isotropic case may be obtained by replacing $\beta_{\perp V}$ with β_V in equation (38). From now on we will no longer explicitly show the ordering in ϵ_β.

Figure 3 shows how the dipole flux surfaces are modified by anisotropic pressure. The dipole flux surfaces are obtained by setting $\psi_V = \psi_0$, where $\psi_0(L)$ is a constant corresponding to the L-values in the range $L = 5$–9. The modified flux surfaces are obtained by setting $\psi_V + \psi_2 = \psi_0$, where ψ_2 is obtained by integrating equation (33) or (36) once with respect to the fast flux variable $\tilde{\psi}$. Assuming $P_\perp \propto |\tilde{\psi}|^{-\alpha}$ yields

$$\psi = \psi_V \left[1 + \frac{\beta_{\perp V}}{2(\alpha - 1)} \right]. \tag{39}$$

As expected the dipole flux surface is pushed outward by the finite pressure. Comparison of Figure 3(a) with 3(b) shows how strong anisotropy causes a flux surface displacement which is more localized near the equator.

Recall that our equilibrium calculation is an asymptotic analysis valid near a given field line, it does not contain global effects such as those due to inner and outer radial boundary conditions, for example. Nevertheless, a comparison of Figure 3 with the global numerical solutions plotted in [*Cheng,* 1992] (see Cheng's Figure 1 at $L = 6$, say) shows reasonable qualitative agreement. We will use the results of our local equilibrium calculation in the eigenmode analysis presented in the following section.

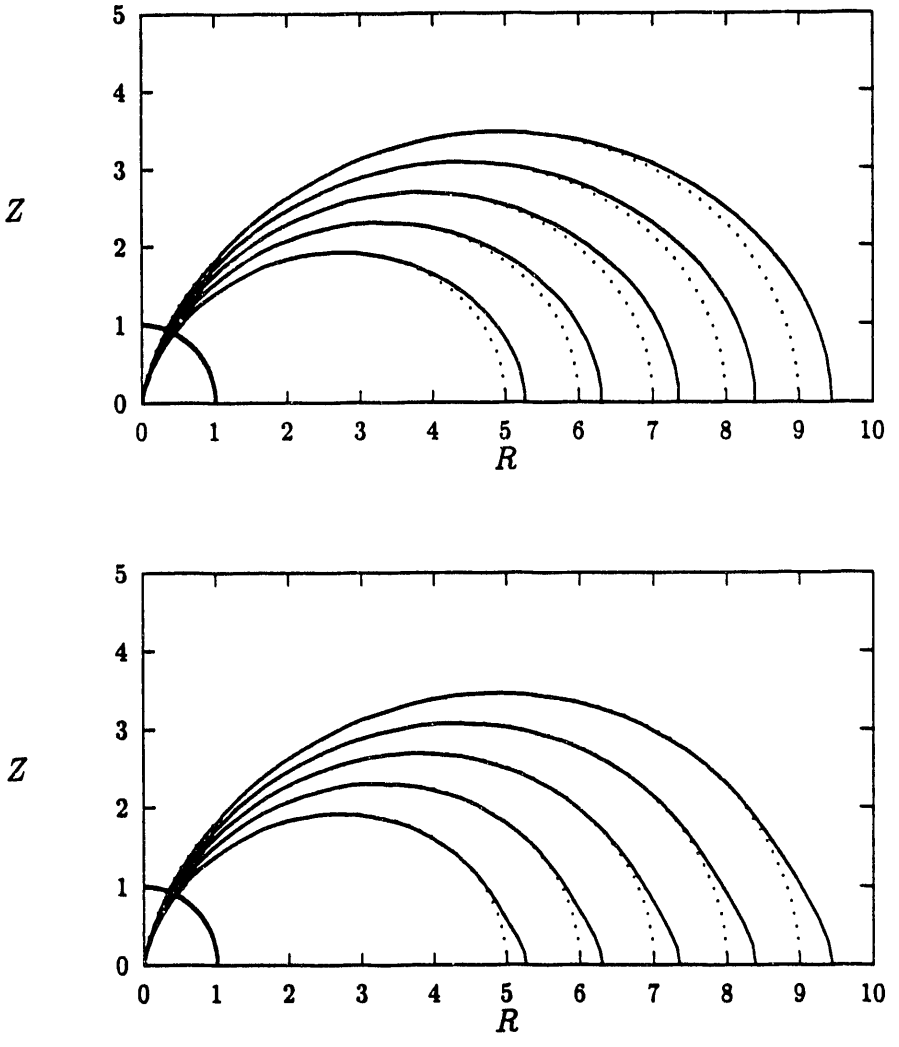

Figure 3: Surfaces of constant flux for $L = 5$–9. The dotted line is the vacuum dipole flux surface and the solid line is the corresponding flux surface obtained from equation (39) with $\beta_{\perp 0V} = 0.5$ and $\alpha = 6$. In (a) $\delta = 0$, corresponding to the isotropic case, and in (b) $\delta_0 = 1 - P_{\|0}/P_{\perp 0} = 0.9$ corresponding to strong anisotropy.

3 Stability of Anisotropic Alfvén-Ballooning Modes

In this section the gyrokinetic eigenmode equations derived in [*Chen and Hasegawa*, 1991] (referred to as CH91 from now on) are used to carry out a linear stability analysis of anisotropic Alfvén-ballooning modes.

3.1 Governing Equations

The gyrokinetic eigenmode equations derived in CH91 take the form of two coupled integro-differential equations to be solved on each equilibrium magnetic field line. One equation is obtained from the perpendicular Ampère's law (CH91 Equation (21)) and the other is a generalized vorticity equation (CH91 Equation (22)). From general properties of the eigenmode equations Chen and Hasegawa concluded that the lowest-frequency antisymmetric mode, commonly called the second harmonic, should be the most unstable mode. Observations [*Takahashi*, 1988] support this conclusion. By "antisymmetric" we mean a wave mode where the transverse electric field component $\delta\mathbf{E}_\perp$ and the compressional magnetic field component $\delta B_\parallel = \mathbf{b}\cdot\delta\mathbf{B}$ have odd symmetry with respect to the geomagnetic equator and the transverse magnetic component $\delta\mathbf{B}_\perp$ has even symmetry. In this paper we restrict our analysis to antisymmetric modes and we focus mainly on the second harmonic. This restriction greatly simplifies the gyrokinetic eigenmode equations of CH91 since several bounce-averaged terms vanish. Furthermore, in order to isolate the fluid effects we neglect all resonant particle terms. Then the perpendicular Ampère's law (CH91 Equation (21)) becomes

$$\tau\,\delta B_\parallel = \frac{4\pi c}{\omega B^2}\left(\mathbf{e}_k\cdot\widetilde{\nabla}P_\perp\right)\,\delta\psi \tag{40}$$

and the generalized vorticity equation (CH91 Equation (22)), becomes

$$B\frac{\partial}{\partial l}\left(\frac{\sigma k_\perp^2}{B}\frac{\partial\,\delta\psi}{\partial l}\right)+\frac{\omega^2 k_\perp^2}{V_A^2}\,\delta\psi = -\frac{4\pi}{B^2}\left(\mathbf{e}_k\cdot\widetilde{\nabla}P_\perp\right)\left(\frac{\omega}{c}\delta B_\parallel+\Omega_B\,\delta\psi\right)$$
$$-\frac{4\pi}{B^2}\left(\mathbf{e}_k\cdot\widetilde{\nabla}P_\parallel\right)\Omega_\kappa\,\delta\psi\,. \tag{41}$$

We now define the notation used in equations (40) and (41). As in the previous section the equilibrium magnetic field is represented as $\mathbf{B}=\nabla\psi\times\nabla\phi$ and σ is the firehose parameter.

The potentials $\delta\phi$, $\delta A_{||} = -(ic/\omega)\partial\,\delta\psi/\partial l$, and $\delta B_{||} = \mathbf{b}\cdot\boldsymbol{\delta}\mathbf{B}$ are all functions of the field line distance l, and are defined in terms of an eikonal form for the wave electromagnetic fields $\boldsymbol{\delta}\mathbf{E}(\mathbf{x},t)$ and $\boldsymbol{\delta}\mathbf{B}(\mathbf{x},t)$ as follows:

$$\delta\phi(\mathbf{x},t) = \delta\phi(l)\,\exp\left(i\int \mathbf{k}_\perp\cdot d\mathbf{x} - i\omega t\right) \tag{42}$$

$$\boldsymbol{\delta}\mathbf{A}(\mathbf{x},t) = \boldsymbol{\delta}\mathbf{A}(l)\,\exp\left(i\int \mathbf{k}_\perp\cdot d\mathbf{x} - i\omega t\right) \tag{43}$$

Here ω is the wave frequency, $\mathbf{k}_\perp(\mathbf{x})$ is the eikonal wave vector, and $\delta\phi(\mathbf{x},t)$ and $\boldsymbol{\delta}\mathbf{A}(\mathbf{x},t)$ are the usual electromagnetic potentials for the wave fields:

$$\boldsymbol{\delta}\mathbf{E}(\mathbf{x},t) = -\nabla\delta\phi(\mathbf{x},t) - \frac{1}{c}\frac{\partial\boldsymbol{\delta}\mathbf{A}(\mathbf{x},t)}{\partial t} \tag{44}$$

$$\boldsymbol{\delta}\mathbf{B}(\mathbf{x},t) = \nabla\times\boldsymbol{\delta}\mathbf{A}(\mathbf{x},t) \tag{45}$$

We will see shortly that it is useful to interpret $\delta\psi$ as a potential function for the transverse (Alfvén) wave components δB_ψ and δE_ϕ. The Coulomb gauge $\nabla\cdot\boldsymbol{\delta}\mathbf{A} = 0$ and the ideal MHD approximation of zero parallel electric field, $\delta E_{||} = 0$, have been used in equations (40) and (41). The latter condition is justified physically by the availability of cold electrons to short out any parallel electric fields. In terms of the potential functions $\delta\psi$ and $\delta\phi$, $\delta E_{||} = 0$ implies $\delta\psi = \delta\phi$. Note that in equations (42)–(45) we have distinguished between a "field line" function (eg., $\delta\psi(l)$) and the corresponding potential (eg., $\delta\psi(\mathbf{x},t)$); in the following we deal only with the field line functions. Finally, in equations (40) and (41)

$$\tau = 1 + \frac{4\pi}{B}\left(\frac{\partial P_\perp}{\partial B}\right)_\psi \tag{46}$$

is the mirror instability parameter ($\tau < 0$ implies mirror instability, see [*Chen and Hasegawa,* 1991]) which is given by

$$\tau = 1 + \beta_\perp\left(1 - \frac{\beta_\perp}{\beta_{||}}\right) \tag{47}$$

for a bi-maxwellian plasma, $\widetilde{\nabla} = \nabla\psi(\partial/\partial\psi)$, $\mathbf{e}_k = \mathbf{k}_\perp\times\mathbf{b}$, $\Omega_B = \mathbf{e}_k\cdot\nabla\ln B$, $\Omega_\kappa = \mathbf{e}_k\cdot\boldsymbol{\kappa}$, where $\boldsymbol{\kappa} = \mathbf{b}\cdot\nabla\mathbf{b}$ is the curvature vector, and $V_A = B/\sqrt{4\pi\rho}$ is the Alfvén speed, where ρ

is the mass density. The wave quantities $\delta\psi$ and $\delta B_{||}$ are regarded as small perturbations on a given equilibrium state.

Equations (40) and (41) describe the coupling between transverse shear-Alfvén modes and compressional slow-magnetosonic modes. The coupling is due to inhomogeneity in the pressure and the magnetic field, as represented by the factors $\mathbf{e}_k \cdot \widetilde{\nabla} P_\perp$, Ω_B, and Ω_κ in equations (40) and (41).

Substituting equation (40) into equation (41) yields

$$B\frac{\partial}{\partial l}\left(\frac{\sigma k_\perp^2}{B}\frac{\partial\,\delta\psi}{\partial l}\right) + \frac{\omega^2 k_\perp^2}{V_A^2}\,\delta\psi + \frac{4\pi}{B^2}\Omega_\kappa \mathbf{e}_k \cdot \widetilde{\nabla}\left(P_{||} + \frac{\sigma}{\tau}P_\perp\right)\,\delta\psi = 0\,, \tag{48}$$

which is a second-order ordinary differential equation in $\delta\psi(l)$. The first term represents field line bending, the second term represents the cold plasma inertia, and the third term is an anisotropic ballooning-interchange term. In this paper we assume stability with respect to interchange modes [*Kadomtsev,* 1963; *Southwood and Kivelson,* 1987] and for brevity we refer to the third term as the ballooning term.

Since the ψ-dependence of $P_{||}$ and $P_\perp$ is mainly determined by the factors $P_{||_0}$ and $P_{\perp 0}$ in equations (12) and (13), the ballooning term can be expressed as

$$\frac{\beta_E k_\phi^2 \kappa_\psi}{L_P}\,\delta\psi, \tag{49}$$

where

$$\beta_E = \frac{1}{2}\left(\beta_{||} + \frac{\sigma}{\tau}\beta_\perp\right), \tag{50}$$

is an effective beta value, k_ϕ is the wavenumber in the azimuthal direction, $\kappa_\psi = \boldsymbol{\kappa} \cdot \widehat{\boldsymbol{\psi}}$ is the curvature component in the $\widehat{\boldsymbol{\psi}} = \nabla\psi/|\nabla\psi|$ direction, and

$$L_P = |\widehat{\boldsymbol{\psi}} \cdot \nabla \ln P_{||}|^{-1} \tag{51}$$

is a radial pressure gradient scale length, which is assumed to be the same for $P_{||}$ and $P_\perp$. On the outer edge of the ring current the parallel and perpendicular pressure gradients and the magnetic curvature vector point in the same direction (Earthward), so the coefficient of $\delta\psi$ in the ballooning term is positive, which is de-stabilizing. Note that the ballooning

term is proportional to k_ϕ^2, while the first two terms in equation (48) are proportional to $k_\perp^2 = k_\phi^2 + k_\psi^2$; thus, in order to calculate the most unstable modes, we assume $k_\phi^2 \gg k_\psi^2$ or $k_\perp^2 \approx k_\phi^2 \equiv m^2/R^2$, where m is the azimuthal mode number. In fact, observations of the transverse wavelengths of magnetospheric hydromagnetic waves [*Takahashi*, 1988] yield azimuthal mode numbers of $m \approx 100$ and a lower bound on the radial wavelengths which implies that $k_\psi^2 \ll k_\phi^2$, consistent with our assumption. Now equation (48) can be rewritten as

$$B\frac{\partial}{\partial l}\left(\frac{\sigma}{BR^2}\frac{\partial \delta\psi}{\partial l}\right) + \frac{\omega^2}{V_A^2 R^2}\delta\psi + \frac{\beta_E \kappa_\psi}{L_P R^2}\delta\psi = 0, \tag{52}$$

which is independent of the azimuthal mode number m. We refer to equation (52) as the anisotropic Alfvén-ballooning equation, it is the basis for our analysis of the effects of finite anisotropic pressure on magnetospheric hydromagnetic waves.

Once boundary conditions are specified the solution of equation (52) becomes a Sturm-Liouville eigenvalue-eigenfunction problem for ω^2 and $\delta\psi(l)$. The boundary conditions we choose are

$$\delta\psi(l_I) = \delta\psi(0) = 0, \tag{53}$$

where $l = 0$ corresponds to the equatorial plane and l_I is the distance from the equator to the ionosphere along a field line. These boundary conditions describe field lines whose ends are tied to a perfectly conducting ionosphere, with field line displacements which have odd symmetry about the equator (assuming North-South symmetry of the equilibrium magnetic field).

Multiplying equation (52) by $\delta\psi$, integrating over the flux tube volume, and using the boundary conditions given in equation (53) we obtain an expression analogous to the well-known MHD Energy Principle [*Bernstein et al.*, 1958], as follows:

$$\omega^2 = \left(\delta W_F + \delta W_B\right)/\delta I\,, \tag{54}$$

where

$$\delta W_F = \int \frac{dl}{B}\frac{\sigma}{R^2}\left(\frac{\partial \delta\psi}{\partial l}\right)^2 \tag{55}$$

is the mass density. The wave quantities $\delta\psi$ and $\delta B_{||}$ are regarded as small perturbations on a given equilibrium state.

Equations (40) and (41) describe the coupling between transverse shear-Alfvén modes and compressional slow-magnetosonic modes. The coupling is due to inhomogeneity in the pressure and the magnetic field, as represented by the factors $\mathbf{e}_k \cdot \widetilde{\nabla} P_\perp$, Ω_B, and Ω_κ in equations (40) and (41).

Substituting equation (40) into equation (41) yields

$$\left(\frac{\sigma k_\perp^2}{B}\frac{\partial\,\delta\psi}{\partial l}\right) + \frac{\omega^2 k_\perp^2}{V_A^2}\,\delta\psi + \frac{4\pi}{B^2}\Omega_\kappa \mathbf{e}_k \cdot \widetilde{\nabla}\left(P_{||} + \frac{\sigma}{\tau}P_\perp\right)\delta\psi = 0\,, \tag{48}$$

which is a second-order ordinary differential equation in $\delta\psi(l)$. The first term represents field line bending, the second term represents the cold plasma inertia, and the third term is an anisotropic ballooning-interchange term. In this paper we assume stability with respect to interchange modes [*Kadomtsev,* 1963; *Southwood and Kivelson,* 1987] and for brevity we refer to the third term as the ballooning term.

Since the ψ-dependence of $P_{||}$ and $P_\perp$ is mainly determined by the factors $P_{||_0}$ and $P_{\perp 0}$ in equations (12) and (13), the ballooning term can be expressed as

$$\frac{\beta_E k_\phi^2 \kappa_\psi}{L_P}\,\delta\psi, \tag{49}$$

where

$$\beta_E = \frac{1}{2}\left(\beta_{||} + \frac{\sigma}{\tau}\beta_\perp\right), \tag{50}$$

is an effective beta value, k_ϕ is the wavenumber in the azimuthal direction, $\kappa_\psi = \boldsymbol{\kappa}\cdot\hat{\boldsymbol{\psi}}$ is the curvature component in the $\hat{\boldsymbol{\psi}} = \nabla\psi/|\nabla\psi|$ direction, and

$$L_P = |\hat{\boldsymbol{\psi}}\cdot\nabla \ln P_{||}|^{-1} \tag{51}$$

is a radial pressure gradient scale length, which is assumed to be the same for $P_{||}$ and $P_\perp$. On the outer edge of the ring current the parallel and perpendicular pressure gradients and the magnetic curvature vector point in the same direction (Earthward), so the coefficient of $\delta\psi$ in the ballooning term is positive, which is de-stabilizing. Note that the ballooning

term is proportional to k_ϕ^2, while the first two terms in equation (48) are proportional to $k_\perp^2 = k_\phi^2 + k_\psi^2$; thus, in order to calculate the most unstable modes, we assume $k_\phi^2 \gg k_\psi^2$ or $k_\perp^2 \approx k_\phi^2 \equiv m^2/R^2$, where m is the azimuthal mode number. In fact, observations of the transverse wavelengths of magnetospheric hydromagnetic waves [*Takahashi*, 1988] yield azimuthal mode numbers of $m \approx 100$ and a lower bound on the radial wavelengths which implies that $k_\psi^2 \ll k_\phi^2$, consistent with our assumption. Now equation (48) can be rewritten as

$$B\frac{\partial}{\partial l}\left(\frac{\sigma}{BR^2}\frac{\partial \delta\psi}{\partial l}\right) + \frac{\omega^2}{V_A^2 R^2}\delta\psi + \frac{\beta_E \kappa_\psi}{L_P R^2}\delta\psi = 0, \tag{52}$$

which is independent of the azimuthal mode number m. We refer to equation (52) as the anisotropic Alfvén-ballooning equation, it is the basis for our analysis of the effects of finite anisotropic pressure on magnetospheric hydromagnetic waves.

Once boundary conditions are specified the solution of equation (52) becomes a Sturm-Liouville eigenvalue-eigenfunction problem for ω^2 and $\delta\psi(l)$. The boundary conditions we choose are

$$\delta\psi(l_I) = \delta\psi(0) = 0, \tag{53}$$

where $l = 0$ corresponds to the equatorial plane and l_I is the distance from the equator to the ionosphere along a field line. These boundary conditions describe field lines whose ends are tied to a perfectly conducting ionosphere, with field line displacements which have odd symmetry about the equator (assuming North-South symmetry of the equilibrium magnetic field).

Multiplying equation (52) by $\delta\psi$, integrating over the flux tube volume, and using the boundary conditions given in equation (53) we obtain an expression analogous to the well-known MHD Energy Principle [*Bernstein et al.*, 1958], as follows:

$$\omega^2 = \left(\delta W_F + \delta W_B\right)/\delta I\,, \tag{54}$$

where

$$\delta W_F = \int \frac{dl}{B}\frac{\sigma}{R^2}\left(\frac{\partial \delta\psi}{\partial l}\right)^2 \tag{55}$$

represents the field line bending contribution to the eigenvalue ω^2,

$$\delta W_B = -\int \frac{dl}{B} \frac{\beta_E \kappa_\psi}{R^2 L_P} \delta\psi^2 \tag{56}$$

represents the ballooning contribution to ω^2, and

$$\delta I = \int \frac{dl}{B} \frac{\delta\psi^2}{R^2 V_A^2} \tag{57}$$

represents the cold plasma inertia. Note the following general properties of equations (54)–(57): (1) If $\sigma > 0$ then $\delta W_F > 0$ and the field line bending contribution is stabilizing. (2) If $\sigma < 0$ we have the firehose instability. (3) As mentioned above, on the outer edge of the ring current the pressure gradient and the field line curvature both point Earthward, so the ballooning contribution δW_B is destabilizing. Even if the plasma is stable with respect to firehose and mirror instabilities (ie., $\sigma > 0$ and $\tau > 0$) a ballooning instability can occur if $|\delta W_B| > \delta W_F$, due to either high beta (large β_E) or steep pressure gradient (small L_P), for example. (4) An interesting special case occurs when $\sigma > 0$ and $\tau \to 0^+$; then $\beta_E \approx (\sigma\beta_\perp/2\tau) \to +\infty$ resulting in $\omega^2 < 0$. We call this case the ballooning-mirror instability.

Now consider the explicit solution of the anisotropic Alfvén-ballooning mode equation, equation (52). Consistent with the multiscale perturbation calculation in the previous section, we evaluate the required equilibrium quantities as follows: The magnetic field **B** is given by equation (38); σ and β_E are given by equations (9) and (50) with $\beta_\parallel$ and $\beta_\perp$ given by equations (15) and (16). All other quantities are evaluated using the vacuum dipole magnetic field. In particular, to evaluate the radial pressure gradient scale length L_P we assume $P_{\parallel 0}$, $P_{\perp 0} \propto L^{-\alpha}$, where L is the dipole L-shell parameter, then equation (51) yields

$$L_P = \frac{\psi_V}{\alpha R B_V} . \tag{58}$$

In order to ensure stability with respect to interchange modes we require that the pressure gradient parameter α satisfy $\alpha \lesssim 20/3$ [*Kadomtsev*, 1963]. Alternatively, from one set of quiet-time observations, Lui *et al* [1992] obtain $\alpha = 3.24 \pm 0.22$, which gives an approximate lower bound on α. We consider values in the range $\alpha \approx 3$–7. Finally, for simplicity

the Alfvén speed $V_A^2 = B^2/4\pi\rho$ is evaluated assuming the mass density ρ is constant along a given field line. Now the anisotropic Alfvén-ballooning equation, together with the boundary conditions in equation (53), can be solved numerically using shooting methods [*Press et al.*, 1986]. A computer code written for this purpose is described in the appendix. The code is called ABC (Alfvén Ballooning Code).

In the following sections we describe numerical results from the ABC code. In all cases we have chosen a field line corresponding to the dipole L-shell $L = 6.6$ (ie., near synchronous orbit). The position of the ionospheric end point of the field line is calculated for a dipole field line intersecting the Earth's surface at $r = 1\mathcal{R}_E$ (ie., the thickness of the ionosphere is neglected). This corresponds to a magnetic latitude of

$$x_I = \cos^{-1}\frac{1}{\sqrt{L}}\,. \tag{59}$$

For $L = 6.6$ $x_I = 67.1°$. Since quantities are normalized to equatorial values (see the appendix) the main effect of varying the L-value is to change the field line length only slightly through equation (59). For example, a range of L-values from $L = 5$–10 results in a change in the normalized field line eigenfrequency of less than about 5% and a corresponding small change in the eigenfunction.

The parallel structure of the eigenmodes is presented by plotting the components of the electromagnetic wave fields $\delta\mathbf{B}(l)$ and $\delta\mathbf{E}(l)$, which are obtained from the source-free Maxwell equations under the orderings and assumptions used in the derivation of the gyrokinetic eigenmode equations as follows:

$$\delta B_\parallel = \frac{k_\phi c}{\omega}\frac{\beta_\perp}{2\tau L_P}\delta\psi\,, \qquad \delta B_\psi = \frac{k_\phi c}{\omega}\frac{\partial\,\delta\psi}{\partial l}\,, \qquad \delta B_\phi = \frac{B}{k_\phi}\frac{\partial}{\partial l}\frac{\delta B_\parallel}{B}\,, \tag{60}$$

and

$$\delta E_\parallel = 0\,, \qquad \delta E_\psi = -\frac{\omega}{k_\phi c}\delta B_\parallel\,, \qquad \delta E_\phi = -ik_\phi\,\delta\psi\,. \tag{61}$$

Note that the components δB_ϕ and δE_ψ are small by a factor of $1/m \approx 1/100$ compared to the other components. Also, in the cold plasma limit ($\beta_\perp = \beta_\parallel = 0$) only the transverse components δB_ψ and δE_ϕ are nonzero and are given by the potential function $\delta\psi$, hence the

interpretation of $\delta\psi$ as representing the transverse shear-Alfvén wave components. Note that when $\delta\psi$ has odd or even symmetry with respect to the geomagnetic equator, by definition the waves modes have the same symmetry.

3.2 The Isotropic Case

It is instructive to consider the isotropic case ($P_{||} = P_{\perp} = P, \quad \sigma = \tau = 1, \quad \beta_{||} = \beta_{\perp} = \beta_E = \beta$) first. Later we will consider the effects of anisotropy as modifications of the isotropic case. For isotropic plasma equation (52) reduces to

$$B\frac{\partial}{\partial l}\left(\frac{1}{R^2B}\frac{\partial\,\delta\psi}{\partial l}\right) + \frac{\omega^2}{R^2V_A^2}\,\delta\psi + \frac{\beta\kappa_\psi}{R^2L_P}\,\delta\psi = 0. \tag{62}$$

This equation has the familiar ballooning mode form [*White,* 1989]; thus, when anisotropy and kinetic effects are neglected, we have the expected result that the gyrokinetic eigenmode equations are equivalent to the linear ideal MHD equations in the ballooning limit. In the next two subsections we consider the effect of increasing β from the cold plasma case, $\beta = 0$, to the finite pressure case with $\beta \approx 1$.

Cold-Plasma Standing Alfvén Waves. When $\beta = 0$ the magnetic field **B** is assumed to be a vacuum dipole field and the Alfvén-ballooning mode equation, equation (62), describes oscillations between the dipole field-line-bending energy and the cold plasma inertia, ie., shear Alfvén waves. Taking into account the boundary conditions, the physical picture of these modes is of standing waves on a nonuniform string. The tension in the string is due to the magnetic field line tension $B^2/8\pi$ and the inertia is provided predominantly by the ions. Note that because $B^2/8\pi$ increases rapidly towards the poles we expect $\delta\psi$, which is proportional to the field line displacement, to be larger near the equator.

The eigenfunctions of the Alfvén-ballooning mode equation are interpreted as the harmonics of this nonuniform string. The eigenfrequencies and plots of the wave components for the first three odd harmonics are given in Figure 4. As discussed in the appendix, the eigenfrequency is normalized to the equatorial Alfvén frequency $\omega_{A0} = V_{A0}/R_0 = B_0/R_0\sqrt{4\pi\rho}$. Note the following properties of the cold plasma harmonics: (1) Since $\beta = 0$ there is no compressional component — the cold plasma harmonics are purely transverse

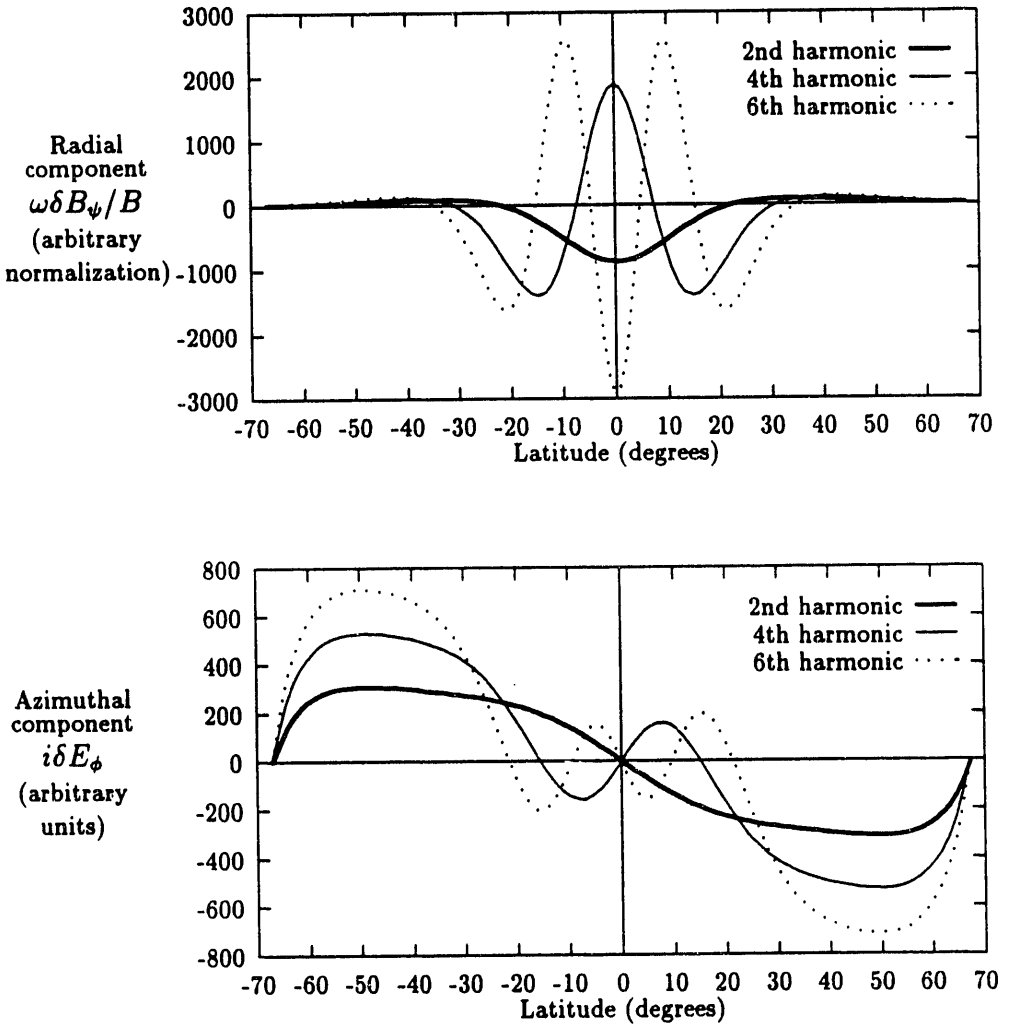

Figure 4: The magnetic and electric wave components for the 2nd, 4th and 6th harmonics (ie., the first three odd eigenmodes) plotted against magnetic latitude along a field line, in the cold-plasma limit. The corresponding eigenfrequencies, normalized to the equatorial Alfvén frequency, are $\omega = 5.49$, 12.53, and 19.48 respectively.

Alfvén waves. (2) As the harmonic number increases the eigenfrequency increases and the number of nodes in the eigenfunction increases (these are general properties of Sturm-Liouville systems). (3) The mode amplitudes are localized near the geomagnetic equator. (4) The eigenvalues and eigenfunctions shown in Figure 4 are consistent with previous solutions in the cold plasma limit, such as the "poloidal modes" considered in [*Cummings et al.*, 1969]. (5) The eigenmode with the lowest frequency (ie., the second harmonic) is the most important for stability considerations since it involves the least field line bending. From now on we focus on properties of the second harmonic.

Finite-Beta Isotropic Alfvén-Ballooning Modes. When finite isotropic plasma pressure is allowed the eigenvalues and eigenfunctions of equation (62) for a given field line depend on two parameters: the radial pressure gradient parameter α, and the equatorial beta value $\beta_0 = 8\pi P/B_0^2$ (or, equivalently, $\beta_{0V} = 8\pi P/B_{0V}^2$ when the vacuum dipole magnetic field is used to calculate the beta value). These two parameters appear as a product in the ballooning term, reflecting the fact that ballooning modes are driven by the pressure *gradient.*

An example of a finite-beta second-harmonic eigenmode solution is shown in Figure 5. Based on Figure 5 and similar plots for a range of parameters, our findings regarding the parallel structure of the finite-β eigenmodes can be summarized as follows: (1) Comparison of Figure 5 with Figure 4 shows that the components $\delta B_\psi/B$ and δE_ϕ are not significantly different for $\beta_{0V} = 0$ and $\beta_{0V} = 0.5$. In general, for a given harmonic the parallel structure of the transverse wave components is insensitive to changes in the beta value. (2) Similarly, the transverse wave components are insensitive to the value of the radial pressure gradient parameter α. Points (1) and (2) are due to the rapid increase of the magnetic tension $B^2/8\pi$ at higher latitudes. (3) There is now a significant compressional component, $\delta B_\parallel$. There are also nonzero δB_ϕ and δE_ψ components, but they are negligibly small and are not shown in Figure 5. Thus, for magnetic latitudes $x \lesssim 10°$, $\delta B_\psi \gg \delta B_\parallel, \delta B_\phi$; ie., near the equatorial plane these modes are predominantly radially polarized. (4) If we plot δB_ψ and δB_ϕ (rather than $\delta B_\psi/B$ and $\delta B_\phi/B$) we find that a node occurs at $x = 20°$ and $x = 11°$,

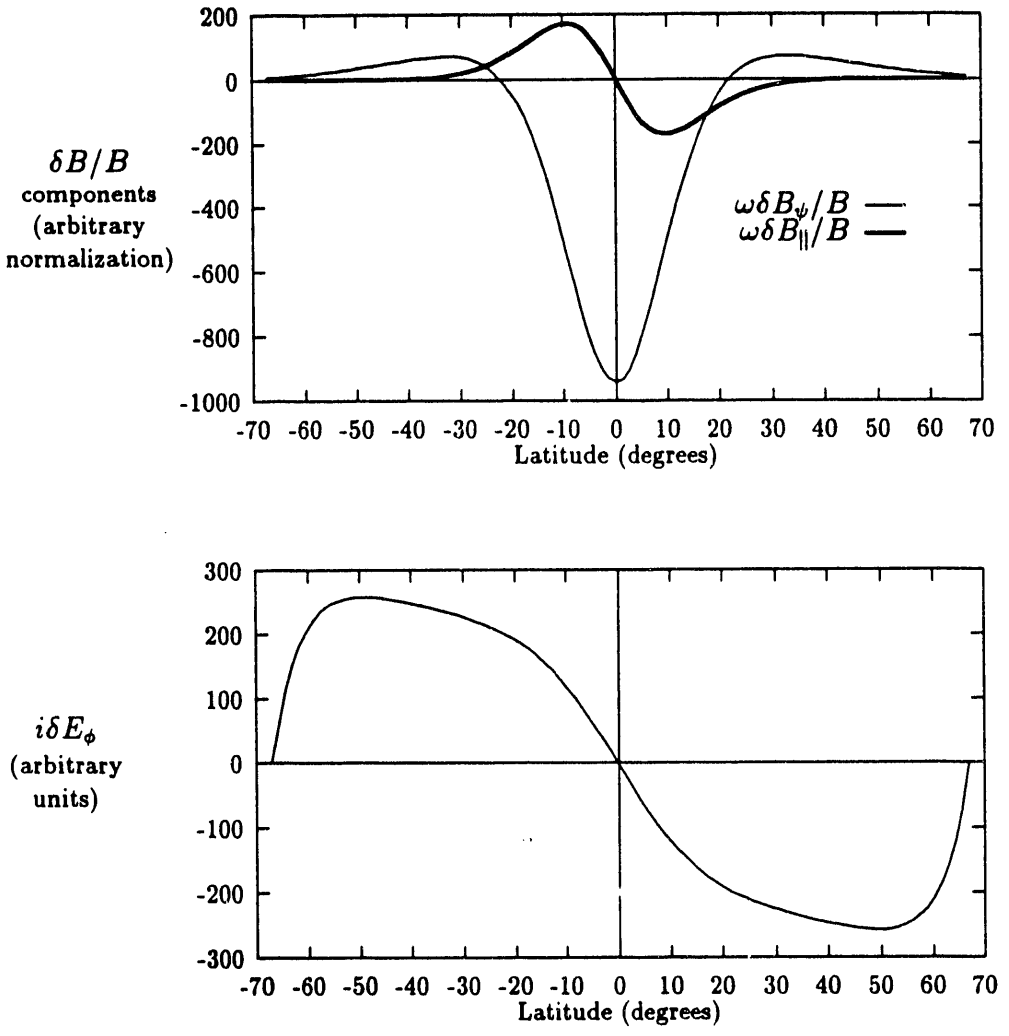

Figure 5: The second-harmonic eigenmode for $L = 6.6$, $\alpha = 6$, $\beta_{0V} = 0.5$, and $m = 100$. The field line eigenfrequency, normalized to the equatorial Alfvén frequency, is $\omega = 4.11$.

respectively. These values are similar to corresponding nodes at $x = 15°$ and $x = 10°$ estimated from near-equatorial spacecraft measurements [*Takahashi et al.*, 1987].

Critical Beta Value for Ballooning Instability. Figure 6 is a plot of the field-line-bending (δW_F) and ballooning (δW_B) contributions to the second harmonic eigenvalue ω^2. As

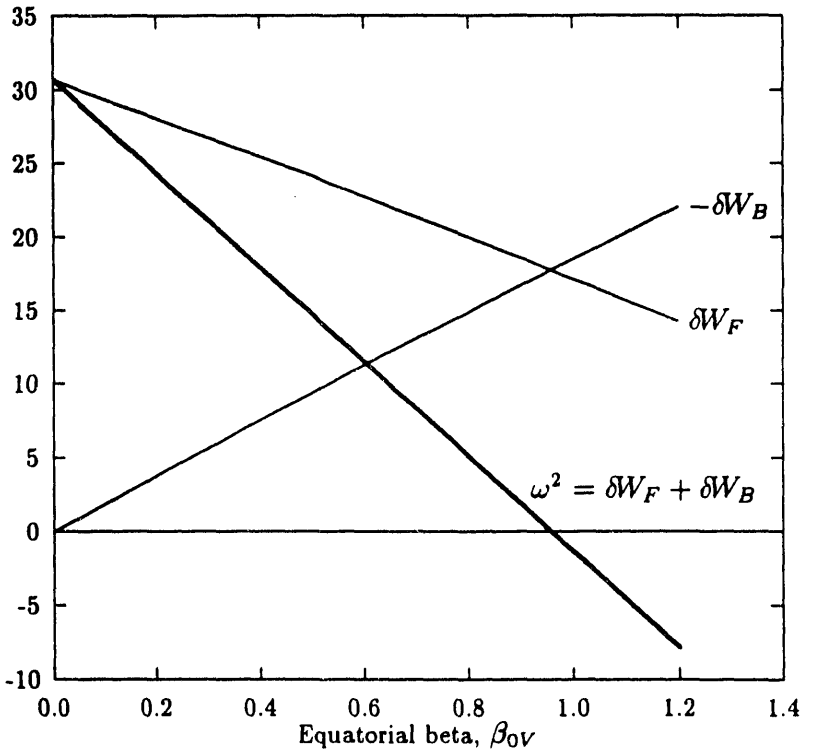

Figure 6: Field-line-bending and ballooning contributions to the second harmonic eigenvalue ω^2. For this plot $L = 6.6$, $\alpha = 6$, and $\delta = 0$. As discussed in the appendix δW_F, δW_B, and ω^2 are normalized so that $\omega^2 = \delta W_F + \delta W_B$ (ie., $\delta I = 1$ in equation (54)) and ω is the field line eigenfrequency in units of the equatorial Alfvén frequency.

the beta value is increased the ballooning contribution increases, the field-line bending contribution decreases, and the square of the wave frequency decreases linearly with β_{0V}.

Note from equation (60) that $\delta B_{\|}/\delta B_{\psi}$ also increases as $\alpha\beta_{0V}$ increases, ie., the wave polarization becomes more compressional. A linear fit to the ω^2 curve in Figure 6 yields

$$\omega^2 = \Omega_0^2 - \Gamma_0\, \beta_{0V}, \tag{63}$$

with $\Omega_0^2 = 30.7$ and $\Gamma_0 = 32.1$. Marginal stability ($\omega^2 = 0$) occurs at the critical value $\beta_{0V}^B = 0.958$. Above this critical value, a reactive-type ($\omega^2 < 0$) MHD ballooning instability results, hence the superscript B on the threshold value β_{0V}^B. Similar plots of ω^2 for pressure gradient parameters of $\alpha = 3$ and $\alpha = 7$ show this linear relationship with $\beta_{0V}^B = 1.33$ and $\beta_{0V}^B = 0.874$ respectively. Thus steeper pressure profiles result in lower threshold values for ballooning instability, as expected [*Chen and Hasegawa,* 1991].

Spacecraft measurements of beta yield a local value, $\beta = 8\pi P/B^2$, rather than the value calculated with the vacuum dipole field, $\beta_V = 8\pi P/B_V^2$. Using equation (38), the local value is related to the vacuum value by

$$\beta = \frac{\beta_V}{(1 - \beta_V/2)^2}\,. \tag{64}$$

Thus the critical value $\beta_{0V}^B = 0.958$ for $\alpha = 6$ corresponds to a local equatorial value of $\beta_0^B = 3.53$, for example. A brief survey of published observations [*Lui et al.,* 1987; *Lui and Hamilton,* 1992] shows $\beta_0 \lesssim 1$, thus the threshold beta-value for isotropic ballooning instability appears to be well above the observed values.

Note that the ϵ_β ordering used in our equilibrium calculation breaks down near the threshold value for ballooning instability. We expect that the results for the eigenmode calculations near threshold are still qualitatively correct, but the numerical value of the threshold beta should be regarded as a rough estimate, valid to within about a factor of two or three.

3.3 Effects of Anisotropy - The β–δ Stability Diagram

We now consider the effect of anisotropic pressure on the stability and the parallel structure of the second harmonic eigenmode. When anisotropic pressure is allowed the solutions of equation (52) for a given field line depend on three parameters: (i) the pressure gradient

parameter α, (ii) a measure of the magnitude of the plasma pressure, for which we choose the average beta value $\overline{\beta} = (1/3)(\beta_{||} + 2\beta_{\perp})$, and (iii) a measure of the plasma anisotropy, for which we choose the anisotropy parameter $\delta = 1 - P_{||}/P_{\perp} = 1 - \beta_{||}/\beta_{\perp}$.

It is useful to summarize the effects of anisotropic pressure on stability with reference to the $\overline{\beta}_0$–δ_0 parameter space, where $\overline{\beta}_0$ is the equatorial average beta value and δ_0 is the equatorial anisotropy parameter. In Figure 7 we have plotted curves in the $\overline{\beta}_0$–δ_0 parameter

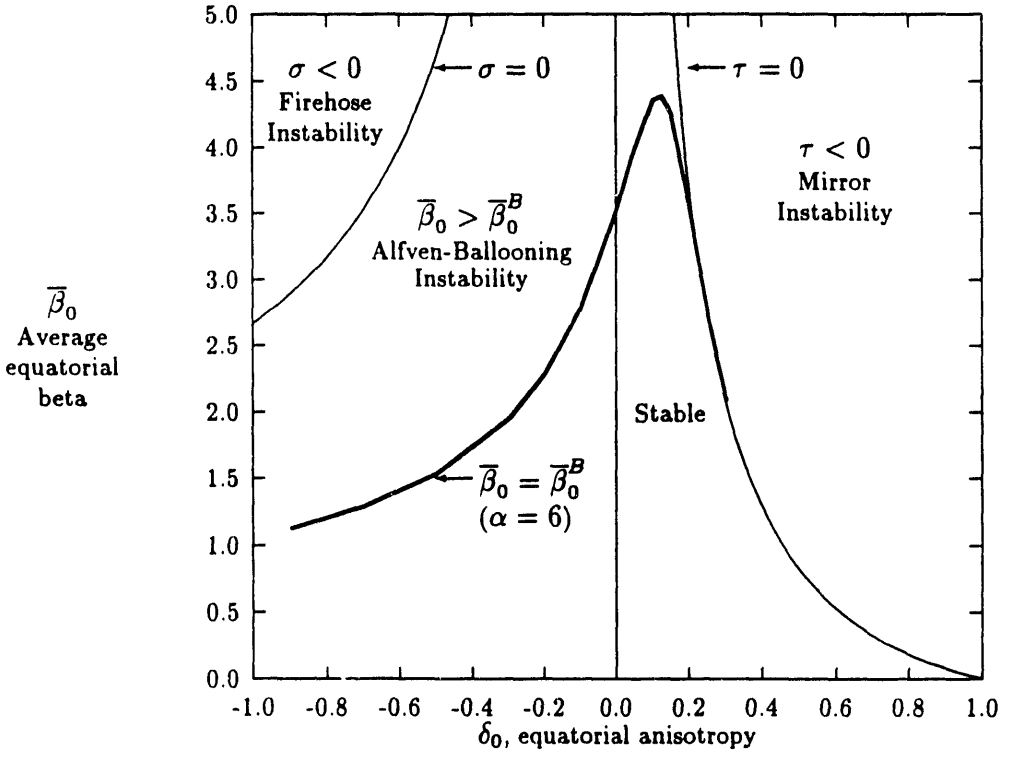

Figure 7: A "β–δ stability diagram". That is, a plot of the instability regions with respect to the $\overline{\beta}_0$–δ_0 parameter space, where $\overline{\beta}_0 = (1/3)(\beta_{||_0} + 2\beta_{\perp_0})$ is the average equatorial beta value and $\delta_0 = 1 - \beta_{||_0}/\beta_{\perp_0}$ is the equatorial anisotropy parameter. For this plot $L = 6.6$ and the ballooning instability threshold ($\overline{\beta}_0 = \overline{\beta}_0^B$) has been calculated for $\alpha = 6$.

space which correspond to the threshold values for the firehose and mirror instabilities (ie., the curves corresponding to $\sigma = 0$ and $\tau = 0$) and the critical beta value $\overline{\beta}_0^B$ for ballooning instability. For brevity we refer to Figure 7 as a "β–δ" stability diagram. We have chosen the beta value $\overline{\beta}_0$ rather than the value calculated with the dipole field $\overline{\beta}_{0V}$ because it is more easily compared with observations. Note the following features of the β–δ stability diagram: (1) The parameter space is divided into four regions corresponding to firehose instability, mirror instability, ballooning instability and a stable region. (2) For very low beta values ($\overline{\beta} \to 0$) the plasma is stable. As $\overline{\beta}$ is increased the plasma becomes unstable to ballooning modes before it reaches the firehose or mirror instabilities, although the ballooning and mirror thresholds converge to the ballooning-mirror threshold for sufficiently large positive anisotropy. (3) Except for a region of mild positive anisotropy (ie., $0 < \delta_0 \lesssim 0.2$ for $\alpha = 6$), the critical beta value for ballooning instability is *lowered* by anisotropy. (4) Observations [*Lui et al.*, 1987; *Lui and Hamilton*, 1992] show typical values of $\beta_0 \lesssim 1$ and $0 \lesssim \delta_0 \lesssim 0.5$, thus, although it appears unlikely that the ballooning instability occurs for isotropic conditions, it may be possible to approach the ballooning-mirror instability threshold shown at $\delta_0 \approx 0.5$ on the β–δ diagram. Note that the ϵ_β ordering used in our equilibrium calculation is valid in this region of parameter space.

In order to better understand the onset of the ballooning instability shown in Figure 7, in Figure 8 we have plotted the beta dependence of the eigenvalue ω^2 and the field-line-bending and ballooning contributions δW_F and δW_B (using equations (54)–(57)) for four values of the anisotropy δ_0. As in Figure 6 the intersection of a δW_F curve and the corresponding δW_B curve occurs at the critical beta value for ballooning instability. From Figure 8 we conclude that, compared with the isotropic case, (1) for negative anisotropy (ie., $\delta_0 < 0$ or $P_\perp < P_\parallel$) the critical beta value for ballooning instability is lowered due to decreased field line bending and increased ballooning destabilization, (2) for mild positive anisotropy (ie., $0 < \delta_0 \lesssim 0.2$ or $P_\perp \gtrsim P_\parallel$) the critical beta value is raised slightly due to the dominance of increased field line bending stabilization, and (3) for strong positive anisotropy (ie., $\delta_0 > 0.2$ or $P_\perp \gg P_\parallel$) the critical beta value is lowered due to the strongly

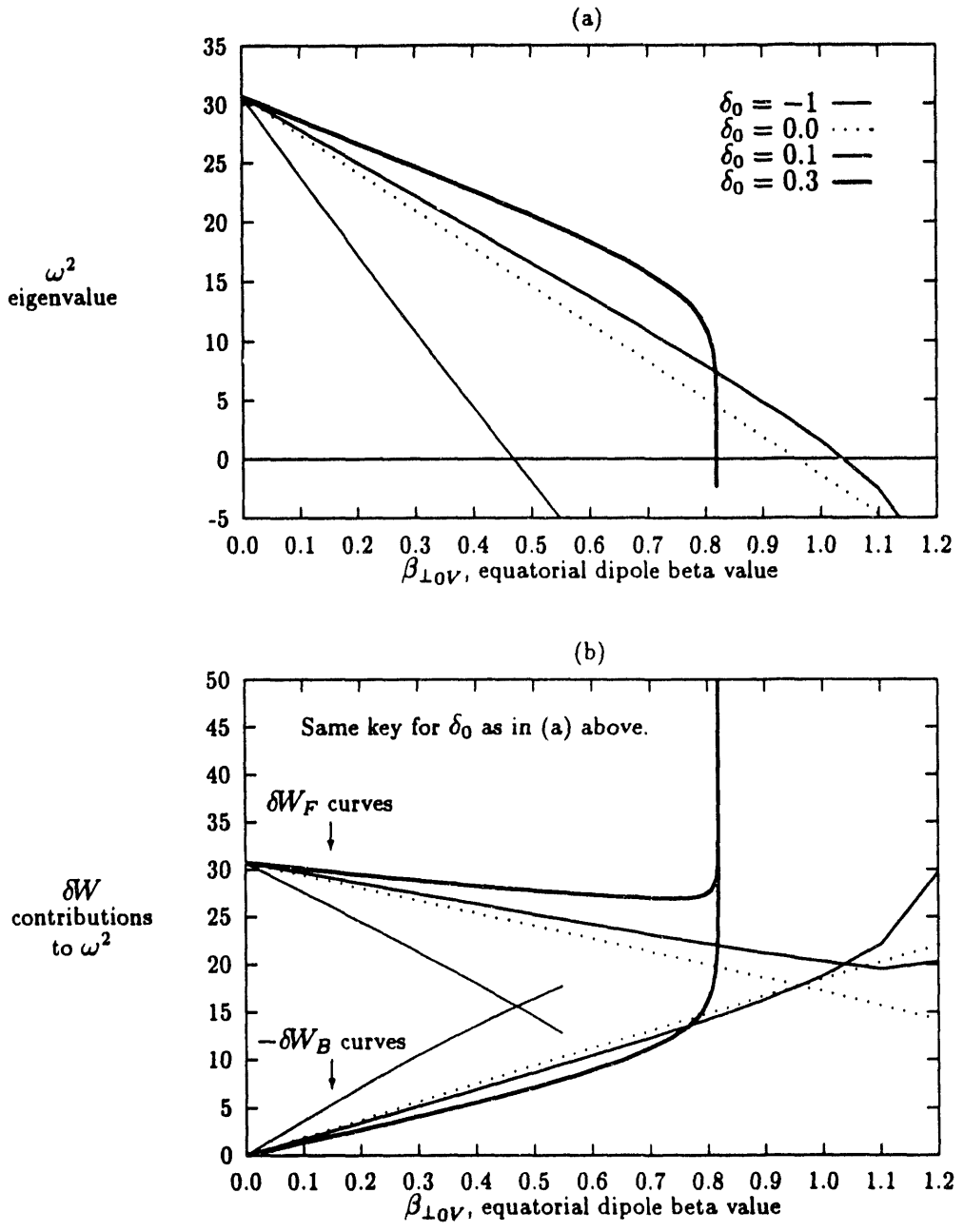

Figure 8: In (a) the normalized eigenvalue ω^2 is plotted versus the equatorial beta value $\beta_{\perp 0V}$ for four values of the equatorial anisotropy δ_0. In (b) the δW_F contribution to ω^2 (the curves starting at the 30.7 when $\beta_{\perp 0V} = 0$) and the δW_B contribution to ω^2 (curves starting at the origin) are plotted for the same four values of δ_0. For these plots $L = 6.6$ and $\alpha = 6$. The normalization is described in the appendix.

increased ballooning-mirror destabilization which occurs in the narrow region corresponding to $\tau \rightarrow 0^+$ (although it is difficult to see in Figure 8, for the $\delta_0 = 0.3$ case $\omega^2 \rightarrow 0$ because δW_B increases more rapidly than δW_F as $\tau \rightarrow 0^+$).

Finally, consider the effect of anisotropy on the parallel structure of the eigenmodes. In Figure 9 we have plotted the transverse and compressional magnetic components for three different values of the equatorial anisotropy. Clearly the effect of anisotropy on the transverse wave component is weak. However, the compressional component $\delta B_{||}$ can be greatly enhanced near the equator due to increasing positive anisotropy. This is especially true when the ballooning-mirror instability threshold is approached since, from equation (60), $\delta B_{||} \propto (\alpha\beta_\perp/2\tau)\,\delta\psi$, which becomes large as $\tau \rightarrow 0^+$; in this case the resulting modes may have a compressional component comparable to or larger than the radial component.

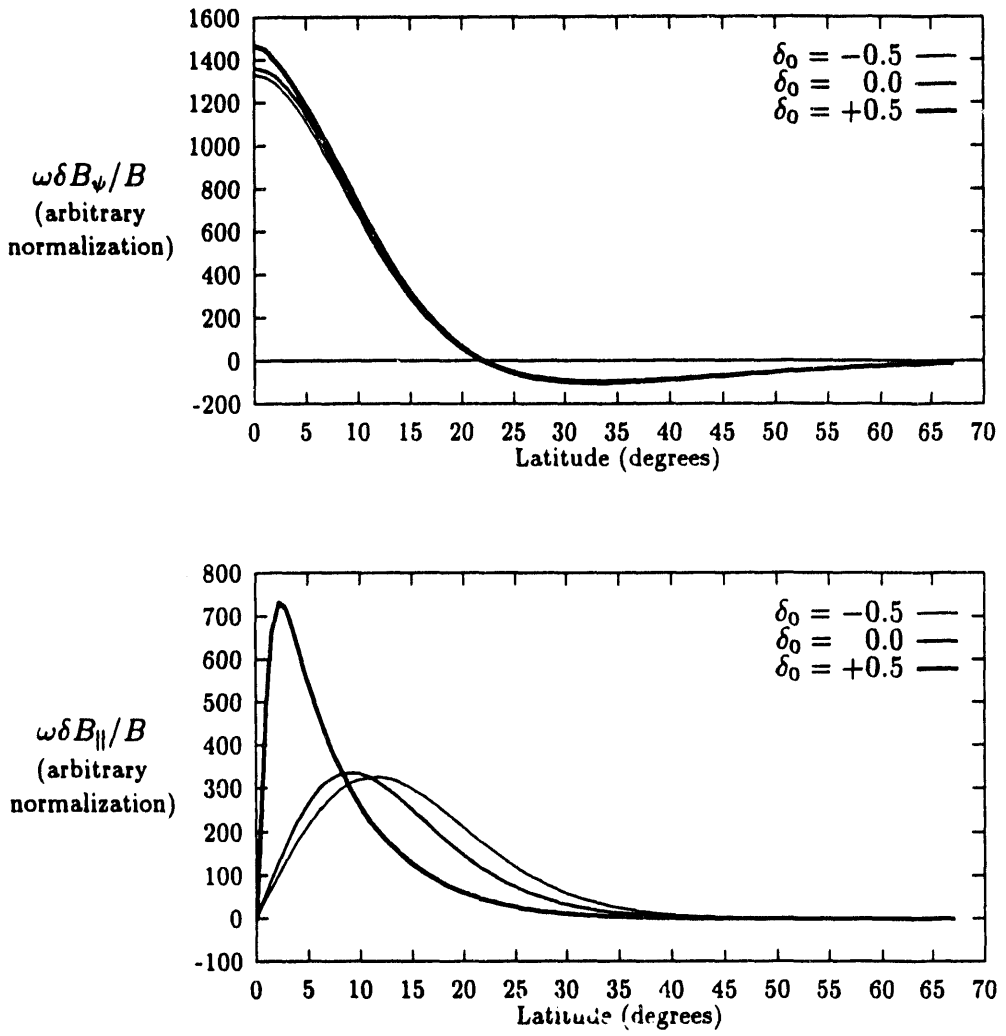

Figure 9: Effects of anisotropy on the transverse (δB_ψ) and compressional ($\delta B_\parallel$) magnetic wave components. For these plots $L = 6.6$, $\alpha = 6$ and $\beta_{\perp 0V} = 0.5$. Recall that δB_ψ is symmetric and $\delta B_\parallel$ is antisymmetric with respect to the equatorial plane.

4 Summary and Discussion

We have carried out a theoretical study of the stability and field-aligned structure of hydromagnetic waves in the Earth's magnetosphere, including effects of finite anisotropic pressure gradients. We have considered regions where geomagnetic field lines are approximately dipolar and where the pressure gradient points Earthward. This corresponds roughly to magnetic field lines which cross the equatorial plane at radial distances between about five and ten Earth radii.

Our formulation is based on the reduced gyrokinetic eigenmode equations of Chen and Hasegawa [1991] but all kinetic effects are neglected in order to focus on the effects of pressure anisotropy on the hydromagnetic modes. The analysis is also restricted to antisymmetric modes and we concentrate mainly on the lowest-frequency antisymmetric harmonic (often called the second harmonic). An approximate analytic solution of the Grad-Shafranov equation for anisotropic MHD equilibrium is obtained. This equilibrium solution is then used to numerically solve the corresponding eigenmode equations. The eigenmode solutions yield the linear properties of coupled shear-Alfvén and slow-magnetoacoustic waves with high azimuthal mode number ($m \gg 1$). Following Chen and Hasegawa [1991] we refer to these modes as anisotropic Alfvén-ballooning modes.

The main results of the anisotropic MHD equilibrium analysis are equations (15) and (16) which describe the field-aligned variation of the parallel and perpendicular beta values (for a locally bi-maxwellian plasma), and equation (38) which describes the local modification of a zero-pressure equilibrium magnetic field due to finite anisotropic pressure. We find that the field-aligned dependence of the plasma pressure becomes more peaked at the equator with increasing anisotropy (see Figure 1). The derivation of equation (38) makes use of the fact that the pressure gradient scale length is small compared to the magnetic field scale length and assumes that the perpendicular beta value calculated using the vacuum dipole field is a small parameter ($\beta_{\perp V} \ll 1$). Note that, from equation (64), $\beta_{\perp V} = 1$ corresponds to a local (measured) beta value of $\beta_\perp = 4$. We expect that our theoretical results for cases where $\beta_{\perp V} \approx 1$ (such as the estimate of the isotropic ballooning threshold)

are qualitatively correct and are probably accurate to within factors of two or three, but this should be tested using a more general equilibrium solution such as that described by Cheng [1992], for example.

The main equations governing the anisotropic Alfvén-ballooning modes are equations (52), (53), (60), and (61). The numerical solution of these equations is described in the Appendix.

For the isotropic pressure case the Alfvén-ballooning modes show the well-known standing wave structure along the field line [*Cummings et al.*, 1969] and their frequency-squared decreases with increasing beta value until they become ballooning unstable at the local equatorial threshold value $\beta_0^B \approx 3.5$. This threshold value is above typical observed equatorial beta values of $\beta_0 \lesssim 1$. In the cold-plasma limit the isotropic modes are purely transverse with dominant wave power in the azimuthal-electric and radial-magnetic wave components. Finite pressure results in a finite compressional component which can become comparable to the radial magnetic component when $\beta_0 \approx 1$, and finite but negligibly small radial-electric and azimuthal-magnetic wave components.

The effects of anisotropy on the linear stability are conveniently summarized in the β–δ diagram, Figure 7. Our main conclusions are: (1) As either the average beta value or the anisotropy is increased from zero the plasma becomes ballooning unstable before it reaches the firehose or mirror instability thresholds. (2) For sufficiently large positive ($P_\perp > P_\parallel$) anisotropy the ballooning and mirror thresholds converge to a "ballooning-mirror" threshold corresponding to $\tau \to 0^+$. (3) Except for a small region of mild positive anisotropy, the critical beta value for ballooning instability is lowered by anisotropy. (4) A brief survey of spacecraft measurements [*Lui et al.*, 1987; *Lui and Hamilton*, 1992] shows that $\overline{\beta}_0 \lesssim 1$ and $P_\perp/P_\parallel \lesssim 2$ have been observed. Comparison of these values with Figure 7 suggests that the ballooning-mirror instability threshold may sometimes be approached in the Earth's magnetosphere. Note that the low-beta ordering used in our equilibrium calculation is valid in this region of parameter space. (5) Compared to the cold-plasma case the field line eigenfrequency can be significantly lowered by finite-pressure effects;

see equation (63) and Figure 8(a). (6) The main effect of finite anisotropy on the wave polarization is a dramatic increase in the compressional magnetic component near the ballooning-mirror instability threshold, as shown in Figure 9.

The β–δ diagram is useful because it organizes the firehose, mirror and ballooning instabilities in an easily understood graphical form. However, it should be noted that the results in this paper represent an approximate calculation of the boundaries between the various instability regions. A more realistic treatment of the distribution function F_0, the ionospheric boundary condition and the radial mode structure is desirable to enable a better comparison with measurements. Furthermore, in the β–δ diagram we have parametrized the various stability regions with respect to the equatorial values of the average beta $\overline{\beta}$ and the anisotropy δ. We emphasize that the instability of the Alfvén-ballooning modes is dependent on the global MHD equilibrium along the field lines and in general a one-point measurement is not sufficient to determine instability. However, we note that with a sufficiently detailed measurement of the local conditions (such as a complete measurement of the equatorial distribution function, for example) one can determine the global equilibrium and the instability conditions can be evaluated.

Finally, a more complete treatment of the linear stability of magnetospheric hydromagnetic waves requires a calculation which includes even modes and the neglected kinetic effects such as particle trapping, wave-particle resonances and finite gyroradius effects. A preliminary calculation [*Chan,* 1991] which includes wave-particle resonances and finite gyroradius effects for antisymmetric modes suggests that Alfvén-ballooning modes may be excited by a magnetic drift-bounce resonance [*Southwood,* 1976; *Chen and Hasegawa,* 1988] at a critical equatorial beta value less than about 10^{-1}, whenever there is an Earthward pressure gradient.

A Numerical Solution of the Anisotropic Alfvén-Ballooning Equation

In this appendix we describe the computer code used to solve equation (52), the anisotropic Alfvén-ballooning equation:

$$B\frac{\partial}{\partial l}\left(\frac{\sigma}{F^2B}\frac{\partial\,\delta\psi}{\partial l}\right)+\frac{\beta_E\kappa_\psi}{R^2L_P}\,\delta\psi+\frac{\omega^2}{R^2V_A^2}\,\delta\psi=0.$$

As outlined in the main body of the paper, we use the results of Section 2 for the multiscale perturbation expansion of the anisotropic Grad-Shafranov equation, discarding terms of order higher than $\mathcal{O}(\epsilon_\beta)$ in the small parameter $\epsilon_\beta \sim \beta_{\perp V}$. Then the distance along the magnetic field line l, the distance from the symmetry axis R, and the curvature κ_ψ can be calculated using the vacuum dipole magnetic field.

The remaining quantities in equation (52) are calculated as follows. Note that the subscript "V" denotes quantities which are evaluated using the vacuum dipole field and the subscript "0" denotes quantities which are evaluated at the equator. Using equation (38) the magnitude of the magnetic field is calculated as

$$B = B_V(1-\tfrac{1}{2}\beta_{\perp V})\,, \tag{65}$$

where, from equation (16),

$$\beta_{\perp V}=\beta_{\perp 0V}\left(\frac{B_{0V}}{B_V}\right)^2\left(\frac{1-\delta_0}{1-\delta_0 B_{0V}/B_V}\right)^2 \tag{66}$$

with $\beta_{\perp 0V}=8\pi P_{\perp 0}/B_{0V}^2$ and $\delta_0 = 1-P_{\|0}/P_{\perp 0}$. Using equations (9) and (11) the firehose parameter is calculated as

$$\sigma = 1+\tfrac{1}{2}\beta_\perp\delta, \tag{67}$$

where δ is given by equation (14) and $\beta_\perp$ is given by equation (16) with

$$\beta_{\perp 0}=\frac{8\pi P_{\perp 0}}{B_0^2}=\frac{\beta_{\perp 0V}}{(1-\frac{1}{2}\beta_{\perp 0V})^2}\,. \tag{68}$$

The effective beta value (equation (50)) is also calculated from δ and $\beta_\perp$ according to

$$\beta_E=\frac{\beta_\perp}{2}\left(1-\delta+\frac{\sigma}{\tau}\right), \tag{69}$$

where the mirror parameter is given by

$$\tau = 1 - \frac{\beta_\perp \delta}{1-\delta}. \tag{70}$$

The pressure gradient scale length L_P is calculated using equation (58) and the Alfvén speed is given by $V_A^2 = B^2/4\pi\rho$ where ρ is the mass density.

Changing variables from field line length l to latitude x and normalizing lengths with $R_N = L\mathcal{R}_E$, magnetic fields with $B_N = B_{0V} = \mathcal{B}_E/L^3$, and velocities with $V_N = B_N/\sqrt{4\pi\rho_0}$, where $\mathcal{R}_E = 6380$ km is the Earth radius, $\mathcal{B}_E = 0.31$ gauss is the magnetic field at the Earth's surface, L is the dipole L-shell parameter and ρ_0 is the equatorial mass density, and denoting normalized quantities by a tilde, the anisotropic Alfvén-ballooning equation becomes

$$\frac{d}{dx}\left(\frac{\sigma}{\tilde{L}_x \tilde{B}\tilde{R}^2}\frac{d\widetilde{\delta\psi}}{dx}\right) + \frac{\tilde{L}_x}{\tilde{B}\tilde{R}^2}\left(\frac{\beta_E \tilde{\kappa}_\psi}{\tilde{L}_P} + \frac{\tilde{\omega}^2}{\tilde{V}_A^2}\right)\widetilde{\delta\psi} = 0, \tag{71}$$

where

$$\tilde{R} = \cos^3 x, \tag{72}$$

$$\tilde{B} = \tilde{B}_V(1 - \tfrac{1}{2}\beta_{\perp V}) \text{ with } \tilde{B}_V = \frac{\sqrt{1+3\sin^2 x}}{\cos^6 x}, \tag{73}$$

$$\tilde{L}_x = \frac{\partial \tilde{l}}{\partial x} = \cos x\sqrt{1+3\sin^2 x}, \tag{74}$$

$$\tilde{\kappa}_\psi = \frac{3(1+\sin^2 x)}{\cos x(1+3\sin^2 x)^{3/2}}, \tag{75}$$

$$\tilde{L}_P = \frac{1}{\alpha}\frac{\cos^3 x}{\sqrt{1+3\sin^2 x}}, \tag{76}$$

and

$$\tilde{V}_A^2 = \frac{\tilde{B}^2}{\rho/\rho_0}. \tag{77}$$

The mass density is assumed to be constant along the field line (ie., $\rho/\rho_0 = 1$).

The NAG shooting-method routine D02KEF [*NAG*, 1982] is used to calculate the eigenvalue $\tilde{\omega}_j^2$ and the eigenfunction $\widetilde{\delta\psi}_j$ for the jth harmonic of equation (71). The computer

code is called ABC (Alfvén Ballooning Code). There is an arbitrary normalization factor implicit in the calculation of the eigenfunction $\widetilde{\delta\psi}_j$; for convenience we choose this factor to make $\widetilde{\delta I}$ of equation (57) equal to unity.

A calculation of $\tilde{\omega}^2$ by numerically evaluating the flux tube integrals in equations (54)–(57) provides a useful way to display the relative contributions of field-line-bending and ballooning terms to the eigenvalue, as in Figure 8 for example. Furthermore, a comparison with the eigenvalue obtained directly from the shooting code provides a check on the internal consistency and numerical accuracy of the shooting code — in all the results presented in this paper the agreement was better than $10^{-4}\%$ of the shooting code value. The flux tube integrals are evaluated numerically using the NAG routine `D01GAF` [*NAG*, 1982].

Acknowledgments. It is a pleasure to thank Mary Hudson and Tony Lui for helpful discussions. This work has been supported by NASA Grant NAGW-1098 and AFOSR Grant F49620-93-1-0101. The work at Princeton is supported by NSF Grant ATM-9211999 and U.S. DoE Contract No. DE-AC02-76-CHO-3073.

REFERENCES

Bender, C. M. and Orszag, S. A. (1978). *Advanced Mathematical Methods for Scientists and Engineers.* International series in pure and applied mathematics. McGraw-Hill Inc.

Bernstein, I. B., Frieman, E. A., Kruskal, M. D., and Kulsrud, R. M. (1958). An energy principle for hydromagnetic stability problems. *Proc. Roy. Soc.*, A244:17–40.

Chan, A. A. (1991). *Interaction of Energetic Ring Current Protons with Magnetospheric Hydromagnetic Waves.* PhD thesis, Princeton University.

Chen, L. and Hasegawa, A. (1988). On magnetospheric hydromagnetic waves excited by energetic ring-current particles. *J. Geophys. Res.*, 93(A8):8763–8767.

Chen, L. and Hasegawa, A. (1991). Kinetic theory of geomagnetic pulsations 1: Internal excitations by energetic particles. *J. Geophys. Res.*, 96(A2):1503–1512.

Cheng, C. Z. (1992). Magnetospheric equilibrium with anisotropic pressure. *J. Geophys. Res.*, 97(A2):1497–1510.

Cummings, W. D., O'Sullivan, R. J., and Coleman Jr, P. J. (1969). Standing Alfvén waves in the magnetosphere. *J. Geophys. Res.*, 74(3):778–793.

Freidberg, J. P. (1982). Ideal magnetohydrodynamic theory of magnetic fusion systems. *Rev. Mod. Phys.*, 54(3):801–902.

Hameiri, E., Laurence, P., and Mond, M. (1991). The ballooning instability in space plasmas. *J. Geophys. Res.*, 96(A2):1513–1526.

Hasegawa, A. and Sato, T. (1989). *Space Plasma Physics. 1: Stationary Processes.* Springer-Verlag.

Kadomtsev, B. B. (1963). *Hydromagnetic stability of a plasma*, volume 2 of *Reviews of Plasma Physics*, chapter 3, page 170. Editor M. A. Leontovich. Consultants Bureau.

Lee, D.-Y. and Wolf, R. A. (1992). Is the Earth's magnetotail balloon unstable? *J. Geophys. Res.*, 97(A12):19251–19257.

Lui, A. T. Y. and Hamilton, D. C. (1992). Radial profiles of quiet-time magnetospheric parame-

ters. *J. Geophys. Res.*, 97:19325–19332.

Lui, A. T. Y., McEntire, R. W., and Krimigis, S. M. (1987). Evolution of the ring current during two geomagnetic storms. *J. Geophys. Res.*, 92(A7):7459–7470.

Miura, A., Ohtani, S., and Tamao, T. (1989). Ballooning instability and structure of diamagnetic hydromagnetic waves in a model magnetosphere. *J. Geophys. Res.*, 94(A11):15231–15242.

NAG (1982). *NAG Fortran Library Manual Mark 9.* Numerical Algorithms Group, NAG Central Office, 7 Banbury Road, Oxford OX26NN, U.K.

Northrop, T. G. (1963). *The Adiabatic Motion of Charged Particles.* Interscience Publishers, New York.

Pokhotelov, O. A., Pilipenko, V. A., Nezlina, Y. M., Woch, J., Kremser, G., Korth, A., and Amata, E. (1986). Excitation of high-β plasma instabilities at the geostationary orbit: Theory and observations. *Planet. Space Sci.*, 34(8):695–712.

Press, W. H., Flannery, B. P., Teukolsky, S. A., and Vetterling, W. T. (1986). *Numerical Recipes: the Art of Scientific Computing.* Cambridge University Press.

Southwood, D. J. (1976). A general approach to low-frequency instability in the ring current plasma. *J. Geophys. Res.*, 81(19):3340–3348.

Southwood, D. J. and Kivelson, M. G. (1987). Magnetospheric interchange instability. *J. Geophys. Res.*, 92:109–116.

Takahashi, K. (1988). Multisatellite studies of ULF waves. *Adv. Space Res.*, 8(9):427–436.

Takahashi, K., Fennel, J. F., Amata, E., and Higbie, P. R. (1987). Field-aligned structure of the storm time Pc 5 wave of November 14-15 1979. *J. Geophys. Res.*, 92(A6):5857–5864.

Viñas, A. F. and Madden, T. R. (1986). Shear flow-ballooning instability as a possible mechanism for hydromagnetic fluctuations. *J. Geophys. Res.*, 91(A2):1519–1528.

White, R. B. (1989). *Theory of Tokamak Plasmas.* North-Holland.

[1]Present address: Dept of Space Physics and Astronomy, Rice University, Houston, Texas

EXTERNAL DISTRIBUTION IN ADDITION TO UC-420

Dr. F. Paoloni, Univ. of Wollongong, AUSTRALIA
Prof. M.H. Brennan, Univ. of Sydney, AUSTRALIA
Plasma Research Lab., Australian Nat. Univ., AUSTRALIA
Prof. I.R. Jones, Flinders Univ, AUSTRALIA
Prof. F. Cap, Inst. for Theoretical Physics, AUSTRIA
Prof. M. Heindler, Institut für Theoretische Physik, AUSTRIA
Prof. M. Goossens, Astronomisch Instituut, BELGIUM
Ecole Royale Militaire, Lab. de Phy. Plasmas, BELGIUM
Commission-European, DG. XII-Fusion Prog., BELGIUM
Prof. R. Boucique, Rijksuniversiteit Gent, BELGIUM
Dr. P.H. Sakanaka, Instituto Fisica, BRAZIL
Instituto Nacional De Pesquisas Especiais-INPE, BRAZIL
Documents Office, Atomic Energy of Canada Ltd., CANADA
Dr. M.P. Bachynski, MPB Technologies, Inc., CANADA
Dr. H.M. Skarsgard, Univ. of Saskatchewan, CANADA
Prof. J. Teichmann, Univ. of Montreal, CANADA
Prof. S.R. Sreenivasan, Univ. of Calgary, CANADA
Prof. T.W. Johnston, INRS-Energie, CANADA
Dr. R. Bolton, Centre canadien de fusion magnétique, CANADA
Dr. C.R. James,, Univ. of Alberta, CANADA
Dr. P. Lukác, Komenského Universzita, CZECHO-SLOVAKIA
The Librarian, Culham Laboratory, ENGLAND
Library, R61, Rutherford Appleton Laboratory, ENGLAND
Mrs. S.A. Hutchinson, JET Library, ENGLAND
Dr. S.C. Sharma, Univ. of South Pacific, FIJI ISLANDS
P. Mähönen, Univ. of Helsinki, FINLAND
Prof. M.N. Bussac, Ecole Polytechnique,, FRANCE
C. Mouttet, Lab. de Physique des Milieux Ionisés, FRANCE
J. Radet, CEN/CADARACHE - Bat 506, FRANCE
Prof. E. Economou, Univ. of Crete, GREECE
Ms. C. Rinni, Univ. of Ioannina, GREECE
Dr. T. Mual, Academy Bibliographic Ser., HONG KONG
Preprint Library, Hungarian Academy of Sci., HUNGARY
Dr. B. DasGupta, Saha Inst. of Nuclear Physics, INDIA
Dr. P. Kaw, Inst. for Plasma Research, INDIA
Dr. P. Rosenau, Israel Inst. of Technology, ISRAEL
Librarian, International Center for Theo Physics, ITALY
Miss C. De Palo, Associazione EURATOM-ENEA , ITALY
Dr. G. Grosso, Istituto di Fisica del Plasma, ITALY
Prof. G. Rostangni, Istituto Gas Ionizzati Del Cnr, ITALY
Dr. H. Yamato, Toshiba Res & Devel Center, JAPAN
Prof. I. Kawakami, Hiroshima Univ., JAPAN
Prof. K. Nishikawa, Hiroshima Univ., JAPAN
Director, Japan Atomic Energy Research Inst., JAPAN
Prof. S. Itoh, Kyushu Univ., JAPAN
Research Info. Ctr., National Instit. for Fusion Science, JAPAN
Prof. S. Tanaka, Kyoto Univ., JAPAN
Library, Kyoto Univ., JAPAN
Prof. N. Inoue, Univ. of Tokyo, JAPAN
Secretary, Plasma Section, Electrotechnical Lab., JAPAN
S. Mori, Technical Advisor, JAERI, JAPAN
Dr. O. Mitarai, Kumamoto Inst. of Technology, JAPAN
J. Hyeon-Sook, Korea Atomic Energy Research Inst., KOREA
D.I. Choi, The Korea Adv. Inst. of Sci. & Tech., KOREA
Prof. B.S. Liley, Univ. of Waikato, NEW ZEALAND
Inst of Physics, Chinese Acad Sci PEOPLE'S REP. OF CHINA
Library, Inst. of Plasma Physics, PEOPLE'S REP. OF CHINA
Tsinghua Univ. Library, PEOPLE'S REPUBLIC OF CHINA
Z. Li, S.W. Inst Physics, PEOPLE'S REPUBLIC OF CHINA
Prof. J.A.C. Cabral, Instituto Superior Tecnico, PORTUGAL
Dr. O. Petrus, AL I CUZA Univ., ROMANIA
Dr. J. de Villiers, Fusion Studies, AEC, S. AFRICA
Prof. M.A. Hellberg, Univ. of Natal, S. AFRICA
Prof. D.E. Kim, Pohang Inst. of Sci. & Tech., SO. KOREA
Prof. C.I.E.M.A.T, Fusion Division Library, SPAIN
Dr. L. Stenflo, Univ. of UMEA, SWEDEN
Library, Royal Inst. of Technology, SWEDEN
Prof. H. Wilhelmson, Chalmers Univ. of Tech., SWEDEN
Centre Phys. Des Plasmas, Ecole Polytech, SWITZERLAND
Bibliotheek, Inst. Voor Plasma-Fysica, THE NETHERLANDS
Asst. Prof. Dr. S. Cakir, Middle East Tech. Univ., TURKEY
Dr. V.A. Glukhikh,Sci. Res. Inst. Electrophys.I Apparatus, USSR
Dr. D.D. Ryutov, Siberian Branch of Academy of Sci., USSR
Dr. G.A. Eliseev, I.V. Kurchatov Inst., USSR
Librarian, The Ukr.SSR Academy of Sciences, USSR
Dr. L.M. Kovrizhnykh, Inst. of General Physics, USSR
Kernforschungsanlage GmbH, Zentralbibliothek, W. GERMANY
Bibliothek, Inst. Für Plasmaforschung, W. GERMANY
Prof. K. Schindler, Ruhr-Universität Bochum, W. GERMANY
Dr. F. Wagner, (ASDEX), Max-Planck-Institut, W. GERMANY
Librarian, Max-Planck-Institut, W. GERMANY
Prof. R.K. Janev, Inst. of Physics, YUGOSLAVIA

DATE
FILMED
8/17/93
END